

# WEATHERING IN A REGOLITH ON THE WERENSKIOLDBREEN GLACIER FOREFIELD (SW SPITSBERGEN). 2. SPECIATION OF Fe, Mn, Pb, Cu AND Zn IN THE CHRONOSEQUENCE

Grzegorz RZEPA<sup>1\*</sup>, Maciej MANECKI<sup>1</sup>, Grzegorz JAKUBSKI<sup>1</sup>,  
Monika KWAŚNIAK-KOMINEK<sup>1</sup>, Jerzy CZERNY<sup>1</sup> & Dorota GÓRNIAK<sup>2</sup>

<sup>1</sup>AGH University of Science and Technology, Faculty of Geology, Geophysics and Environmental Protection,  
Department of Mineralogy, Petrography and Geochemistry, al. Mickiewicza 30, 30-059 Kraków, Poland;  
e-mails: [gprzepa@cyf-kr.edu.pl](mailto:gprzepa@cyf-kr.edu.pl), [gpmmanec@cyf-kr.edu.pl](mailto:gpmmanec@cyf-kr.edu.pl), [g.jakubski@gmail.com](mailto:g.jakubski@gmail.com),  
[monika.kwasniak@gmail.com](mailto:monika.kwasniak@gmail.com), [jczerny@agh.edu.pl](mailto:jczerny@agh.edu.pl)

<sup>2</sup>University of Warmia and Mazury in Olsztyn, Faculty of Biology and Biotechnology,  
Department of Microbiology, Oczapowskiego 1a, 10-917, Olsztyn, Poland;  
e-mail: [gorniak@uwm.edu.pl](mailto:gorniak@uwm.edu.pl)

\* Corresponding author

Rzepa, G., Manecki, M., Jakubski, G., Kwaśniak-Kominek, M., Czerny, J. & Górniak, D., 2019. Weathering in a regolith on the Werenskioldbreen Glacier forefield (SW Spitsbergen). 2. Speciation of Fe, Mn, Pb, Cu and Zn in the chronosequence. *Annales Societatis Geologorum Poloniae*, 89: 317–341.

**Abstract:** The evolution of chemical speciation of Fe, Mn, Pb, Cu, and Zn was investigated in the chronosequence of young sediments, exposed by a currently retreating Arctic glacier on Spitsbergen. Werenskioldbreen is a 27 km<sup>2</sup> subpolar, land-terminated, polythermal glacier in recession, located near the SW coast of West Spitsbergen. Three samples of structureless till were collected at locations exposed for 5, 45 and 70 years. Four grain-size fractions were separated: > 63, 20–63, 2–20, and < 2 μm. Speciation of Fe, Mn, Pb, Cu, and Zn was determined using a 6-step sequential chemical extraction method: 1) 1 M sodium acetate, 2) 1 M hydroxylamine hydrochloride in acetic acid, 3) sodium dithionite in buffer, 4) acid ammonium oxalate, 5) boiling HCl, 6) residuum. The weathering in the proglacial area of the retreating glacier is very fast. The geochemical fates of the metals in question correlate with each other, reflecting a) the geochemical similarities between them, b) the similarities of their primary mineral sources, c) the significant role of incongruent dissolution. The weathering processes dominating the system are redox reactions and incongruent dissolution, followed by precipitation of secondary phases and partial sorption of aqueous species. As a result, the elements released from weathering minerals are only partially transported away from the system. The remaining part transforms by weathering from the coarse-grained fraction (dominated by fragments of primary minerals) into the fine-grained fraction (in the form of secondary, authigenic minerals or as species sorbed onto a mineral skeleton). This is very strongly pronounced within the chronosequence: the content of each of the metals studied correlates identically with the grain size, despite the differences in their chemical character and affinities. The microscope study presented herein indicates that the role of incongruent dissolution previously was underestimated. Also, the formation of coatings of secondary phases on primary mineral surfaces was observed. All these rapid weathering processes affect the mineral speciation of initial soils as well as the composition of mineral suspensions transported away by rivers to the nearby ocean.

**Key words:** Retreating glaciers, incongruent dissolution, sequential chemical extraction, global warming.

*Manuscript received 18 December 2018, accepted 15 June 2019*

## INTRODUCTION

In the Arctic, the average annual temperature has approximately doubled over the last 100 years, when compared to the average world temperature (Pachauri *et al.*, 2014). A mean global surface warming of up to ca. 5 °C above the 1986–2005 mean is predicted up to 2100 (Collins

*et al.*, 2013). Even higher temperature increase is expected in polar regions (Olsen *et al.*, 2011; Osuch and Wawrzyniak, 2016). A spectacular consequence of global warming is the reduction of ice cover on the Earth's surface, which appears to be accelerating in the 21<sup>st</sup> century (Zemp *et al.*, 2015).

Local mountain glaciers located in lower latitudes at high altitudes are disappearing, as are the ice sheets and continental glaciers in the Arctic regions. The annual mean sea ice extent in the Arctic decreases by approximately 4% per decade (Pachauri *et al.*, 2014).

The retreat of the glaciers results in the uncovering of sediments very susceptible to weathering. The exposed minerals and rocks in these areas decompose relatively fast, reacting with water, air and the biosphere. This is a very important issue because the chemical weathering of continental rocks plays a crucial role as both long-term and short-term regulating factors in the global carbon cycle, and therefore, in the Earth's climate (e.g., Walker *et al.*, 1981; Berner *et al.*, 1983; Beaulieu *et al.*, 2012; Dosseto *et al.*, 2015; Taylor *et al.*, 2016). However, owing to the heterogeneity of the system, complex mineralogy and microbial contribution, our knowledge of the reactions and alteration rates is still far from perfect. Intensive mineralogical and geochemical research has been undertaken in chronosequences at a number of locations worldwide (see for example Mavris *et al.*, 2010, 2011; Kiczka *et al.*, 2011; Dahms *et al.*, 2012; Wojcik *et al.*, 2017; and references therein). Glacier melting results also in an increased outflow of fresh water to coastal, oceanic regions (Shepherd *et al.*, 2012). The meltwaters, enriched in dissolved and suspended constituents derived from chemical weathering on the glacier forefields, are important sources of nutrients supplied into the polar ocean (Wadham *et al.*, 2013; Hawking *et al.*, 2015, 2017; Arrigo *et al.*, 2017; Overeem *et al.*, 2017). Glacial floods related to geothermal activity can give a similar effect (Gałeczka *et al.*, 2015). Therefore, highly productive CO<sub>2</sub>-consuming ecosystems develop in the coastal waters surrounding ice sheets (Rysgaard *et al.*, 2012; Death *et al.*, 2014; Hawking *et al.*, 2014; Sharp and Tranter, 2017).

One of the most important nutrients is iron, which is known to limit the primary production of the oceans (e.g., Boyd *et al.*, 2007; Raiswell, 2011a). The uptake and utilization of Fe by micro-organisms links iron (bio)geochemistry to the global carbon cycle (e.g., Martinez-Garcia *et al.*, 2014). Fe is transferred from the continents to the ocean as particulate matter rather than as dissolved species (Poulton and Raiswell, 2002; Raiswell *et al.*, 2006; Raiswell, 2011a; Bhatia *et al.*, 2013). The major forms of particulate Fe, i.e., clay minerals and iron (oxyhydr)oxides, are hardly soluble in seawater, which limits the bioavailability (Liu and Milleo, 2002; Taylor and Konhauser, 2011). The bioavailability of (oxyhydr)oxides depends on particular mineral species: nanocrystalline ferrihydrite is thought to deliver bioavailable, "highly reactive" iron, whereas the more crystalline goethite and hematite are not reactive (Raiswell, 2011b; Raiswell and Canfield, 2012; Hirst *et al.*, 2017). In general, Fe(II) species are thought to be bioavailable in marine environments (Shoenfelt *et al.*, 2017; Hawking *et al.*, 2018). Many recent studies have shown that ice sheets, both Arctic and Antarctic, are globally significant sources of Fe-bearing (nano)particles, including those potentially bioavailable (e.g., Raiswell, 2011b; Bhatia *et al.*, 2013; Raiswell *et al.*, 2016; Hawking *et al.*, 2014, 2018). A significant source of iron-bearing particulates to the marine environments are glacial meltwaters, rich in suspended sediments, and a por-

tion of these sediments originates from the fluvial reworking of regolith, freshly exposed to weathering by retreating glaciers. Besides iron, the regolith may deliver numerous other chemical constituents, including various trace elements.

In this work, the evolution of chemical speciation of iron and selected trace elements in the chronosequence of young sediments, exposed by a currently retreating Arctic glacier on Spitsbergen, is presented. The authors formulate the hypothesis that the alteration processes in the freshly exposed regolith are very rapid and lead to a sudden release of some elements to solutions and/or to suspensions. Very few geological processes have a time scale similar to the rapid changes observed here. An understanding of these early fast alterations will enable an appreciation of the mechanisms involved in the formation of initial glacial soils in the Arctic climate. This knowledge contributes to a more comprehensive assessment of the response of the global Earth system to rapid climate change.

## STUDY AREA

The Werenskiold Glacier is located in Wedel Jarlsberg Land, near the SW coast of West Spitsbergen (Fig. 1). It is a subpolar land-terminated polythermal glacier, 27 km<sup>2</sup> in area (Pälli *et al.*, 2003), typical of this region of Svalbard (Hagen *et al.*, 1993). The area is under the influence of a suboceanic arctic climate, with an average annual temperature of -4.3 °C and precipitation of 434 mm (Marsz and Styszyńska, 2013). The glacier elevation ranges from 60 to 650 m a.s.l., and its thickness is approximately 235 m (Hagen *et al.*, 1993; Ignatiuk and Migala, 2013). A cold ice surface layer, up to 100 m thick, is underlain by temperate ice<sup>1</sup> (Pälli *et al.*, 2003). The relatively flat proglacial zone of the glacier is surrounded by elevated lateral and terminal moraines (Zwoliński *et al.*, 2013). The moraines are only locally covered with soils. Soils currently forming in the forefield of the Werenskiold Glacier are in the initial stage of development and have poorly developed horizons due to an excessive frost-induced mixing of the surface layer and relatively low intensity of soil mineral weathering (Skiba *et al.*, 2002). The soils thaw in the summer and the permafrost layer starts at a depth of ca. 100 cm below ground level (Kabała and Zapart, 2012). The till, in most cases, is structureless in a pedological sense, often greenish grey and gleyed, owing to continuous saturation with water (Kabała and Zapart, 2009).

The geology of this area was described in detail by Czerny *et al.* (1993). The rocks covered by the Werenskiold Glacier consist of a metasedimentary-metavolcanic polymetamorphic sequence, with a protolith Mesoproterozoic in age. The succession includes mostly the Deilegga Formation, the Eimfjellet Formation, the Jens Erikfjellet Formation and the Vimsodden Formation and was subjected to amphibolite facies metamorphism of the Late Cryogenian (ca. 640 Ma), followed by greenschist facies

<sup>1</sup> Cold ice does not contain any water below the pressure-melting point, whereas temperate ice is a mixture of porous ice and liquid water at the melting temperature (Meyer and Minchew, 2018; Reinardy *et al.*, 2019).

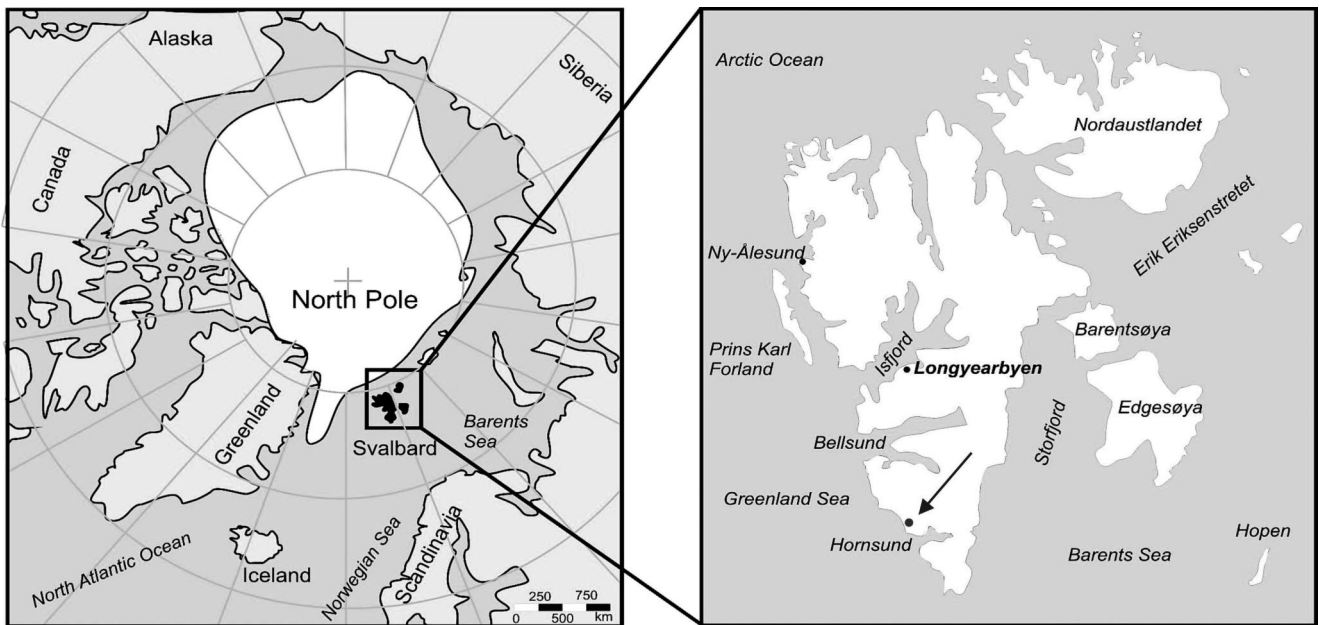


**Fig. 1.** Location of Svalbard in the High Arctic. The arrow indicates the position of Werenskioldbreen (after Kwaśniak-Kominek *et al.*, 2016). Detailed information on sampling sites can be found in Kwaśniak-Kominek *et al.* (2016).

Caledonian metamorphism (Maneck *et al.*, 1998; Majka *et al.*, 2008, 2010, 2013). A major regional dislocation zone cuts across underneath the glacier from Vimsodden through Kosibasset (Czerny *et al.*, 1992a). The variable lithology consists mostly of phyllites, carbonate- and quartz-carbonate-mica schists, chlorite schists, conglomerates, amphibolites, greenschists, and marbles. Carbonate minerals include calcite, dolomite, ankerite and siderite. Polymetallic mineralization layers with Fe, Cu, Pb and Zn sulphides locally are seen along the dislocation zone (Kieres and Piestrzyński, 1992; Czerny *et al.*, 1992b).

The Werenskioldbreen is an excellent example of a fast-retreating glacier. Its recession, which started more than a hundred years ago, reached approximately 25 m per year at the beginning of 21st century (Bukowska-Jania, 2003). Similar phenomena have been observed in the neighbouring areas (Marszałek and Górniak, 2017). Field observations suggest that the regression has accelerated in the past decade, which might be supported by a declining trend in the size of icing fields reported in the Kaffiøyra region (Sobota, 2016) as well as a thinning of the snow cover in the Hornsund area (Laska *et al.*, 2017). The active hydrological season in the area, which spanned previously from June to the beginning of October, was observed to lengthen recently by over a month and lasts from mid-May to late October (Majchrowska *et al.*, 2015).

The analyses of the Werenskioldbreen meltwaters (Stachnik *et al.*, 2016) as well as a complementary mineralogical study, combined with hydrogeochemical modelling of the pore waters in the glacier forefield (Kwaśniak-Kominek *et al.*, 2016), revealed that sulphide oxidation coupled with carbonate dissolution are the dominating processes affecting water chemistry. The contribution of (alumino)silicate weathering and precipitation of secondary phases is smaller. The weathering processes are microbially mediated (Gór-

niak *et al.*, 2017). The spatial changes in pore water and initial soil properties, including nutrient availability, organic matter content, granulation and age, affect microbial community abundance and structure (Górniak *et al.*, 2017). The weathering results in an increase of water mineralization and the evolution of water composition from carbonate-dominated to sulphate-dominated with increasing distance from the glacier.

## MATERIALS AND METHODS

Three samples of initial soils were collected from the Werenskioldbreen forefield in June 2010 (Fig. 1). The samples were named with reference to the distance to the glacier terminus, as C (close, approximately 20 m in 2010), M (middle, approximately 950 m from the terminus), and F (far, approximately 1700 m from the terminus). Their locations correlate with the time of exposure, which was approximately 5, 45 and 70 years, respectively. More details on sampling and sample locations can be found in Kwaśniak-Kominek *et al.* (2016). The sampled sediment is composed predominantly of glacially reworked, primary, rock-forming minerals from the rocks present in the area and include quartz, Na-rich plagioclases, amphiboles, phyllosilicates (micas, chlorites), epidote, carbonates (calcite, dolomite, siderite) and sulphides (pyrite, chalcopyrite, galena, sphalerite). Goethite and secondary (mixed-layered) clays are also present in M and F samples (Kwaśniak-Kominek *et al.*, 2016).

The samples were air-dried, homogenized and gently crushed to pass through a 2-mm sieve. The > 63 µm fraction was obtained by wet sieving. The fine-grained fractions (i.e., 20–63 µm, 2–20 µm, and < 2 µm) were separated by settling in double distilled water. Settling times were calculated according to Stokes law on the basis of the specific densities estimated previously using a pycnometer.

The micromorphology of mineral grains was characterized using scanning electron microscopy (FEI Quanta 200 field emission microscope, operating at 20 kV). Energy dispersive X-ray spectrometry was used for standardless semi-quantitative elemental analyses. All samples were analyzed in a low-vacuum mode without coating.

Speciation of iron, manganese and selected trace elements (zinc, lead, and copper) was determined using a multi-step sequential chemical extraction method. This method has been applied successfully to glacial sediments (Poulton and Canfield, 2005). The experiments were carried out in 50 mL polypropylene centrifuge tubes with a sample size of 0.4 g. After each extraction, the samples were centrifuged at 4500 r.p.m. for 10 min. The concentration of metals was determined in supernatants using a GBC SavantAA atomic absorption spectrometer. At each extraction step, a blank sample was prepared and the standard solutions for AAS were prepared in the matrix of the reagents applied in a particular extraction. The following extraction steps were used:

(1) 1 M sodium acetate ( $\text{CH}_3\text{COONa}$ ) for 48 hours at 50 °C. The pH was adjusted to 4.5 with acetic acid ( $\text{CH}_3\text{COOH}$ ). The reagent selectively dissolves carbonates and removes metals from ion-exchangeable positions (Tessier *et al.*, 1979). Prolonged reaction time and elevated temperature were applied because crystalline siderite and/or ankerite are present in the samples, which are hardly soluble at room temperature (Poulton and Canfield, 2005);

(2) 1 M hydroxylamine hydrochloride ( $\text{HONH}_2 \cdot \text{HCl}$ ) dissolved in 25 % acetic acid. The reagent dissolves “easily reducible” iron oxyhydroxides, i.e., ferrihydrite and lepidocrocite as well as schwertmannite and manganese oxides (Chester and Hughes, 1967; Ross and Wang, 1993). The extraction was carried out for 48 h at room temperature;

(3) Sodium dithionite ( $\text{Na}_2\text{S}_2\text{O}_4$ ) buffered at pH 4.8 with 0.35 M acetic acid and 0.2 M sodium citrate  $\text{C}_3\text{H}_4(\text{OH})(\text{COONa})_3$ . So-called “reducible” iron (oxyhydr)oxides (goethite, hematite and akaganéite) are selectively extracted at this stage (Mehra and Jackson, 1960; Rzepa *et al.*, 2006);

(4) Acid ammonium oxalate: 0.2 M  $(\text{COONH}_4)_2$  and 0.2 M  $(\text{COOH})_2$  at pH 3.0. This reagent is usually used for the selective extraction of ferrihydrite from soils and sediments (Cornell and Schwertmann, 2003). Here it was applied for the extraction of magnetite, since the oxide is also dissolved in the oxalate buffer (Ross and Wang, 1993) and ferrihydrite had been removed already at step (2);

(5) Concentrated (12 M) boiling hydrochloric acid (HCl). It was shown (Raiswell *et al.*, 1994) that the acid extracts metals from some phyllosilicates (nontronite, biotite and chlorite).

(6) The residual fraction including species which had not been dissolved in the previous steps. The extraction involves digestion by a mixture of hot concentrated hydrofluoric (HF), nitric ( $\text{HNO}_3$ ) and perchloric ( $\text{HClO}_4$ ) acids, followed by a treatment with boiling hydrochloric acid. A similar procedure has been previously applied to the “total” extraction of Fe from sediments (Raiswell *et al.*, 2006).

## RESULTS AND DISCUSSION

### Iron

The total iron concentrations vary significantly in the soils studied. In samples M and F, collected far from the glacier terminus, the iron content increases in the fine fraction (Fig. 2): the coarsest fractions ( $> 63 \mu\text{m}$ ) of samples M and F contain 4.2 and 3.7 wt.% Fe, respectively, whereas the finest fraction ( $< 2 \mu\text{m}$ ) contains 7.8 and 12.3 wt.% Fe, respectively (Table 1). A similar trend previously was found in various sediments (Douglas *et al.*, 1999; Singh *et al.*, 1999), including the sediments from glacial meltwaters (Poulton and Raiswell, 2005), the soils of Belyi Island (Moskovchenko *et al.*, 2017), and the soil surface horizons from the nearby Hornsund area (Szymański *et al.*, 2015, 2016). An opposite trend is noticed in the case of sample C, collected close to the glacier front (Fig. 2). Here, in general, more iron occurs in the coarser fractions ( $> 63 \mu\text{m}$  and 20–63  $\mu\text{m}$ ). This means that the total content of Fe in the coarser fractions decreases with the distance from the glacier terminus – from 6.3 wt.% to 3.7 wt.% in the fraction  $> 63 \mu\text{m}$  and from 7.4 wt.% to 3.7 wt.% in the fraction of 20–63  $\mu\text{m}$  (Table 1). The opposite trend is apparent for the finer (2–20  $\mu\text{m}$  and  $< 2 \mu\text{m}$ ) fractions (Fig. 3): there is more iron in the sample F (8.2 wt.% in the fraction of 2–20  $\mu\text{m}$  and as high as 12.3 wt.% in the fraction  $< 2 \mu\text{m}$ ) than in sample M (4.9 wt.% and 7.9 wt.%, respectively) and in sample C (2.8 wt.% and 3.9 wt.%, respectively). These patterns can be explained by higher concentrations of Fe-bearing primary minerals (unweathered silicates, sulphides and carbonates in the very young sediments) in the vicinity of the glacier. At the locations further from the glacier, the minerals have been exposed longer and therefore are affected more by physical and chemical weathering, which alters the mineral speciation of Fe. This is also consistent with the grain-size distribution and the domination of coarse fractions closer to the glacier front (Kwaśniak-Kominek *et al.*, 2016). A similar decrease in the total iron content previously was observed by Pirożnikow and Górniak (1992).

This pattern of total Fe content is supported by the distribution of Fe speciation. In the coarsest ( $> 63 \mu\text{m}$ ) fraction (Fig. 3), the content of “residual” iron is much higher than the “labile” Fe and than the iron extractable from phyllosilicates (i.e., easily extractable at steps 1–4 as well as step 5). The highest dominance of the residuum is apparent in sample C.

The opposite is observed in the finer fractions, particularly in the fraction  $< 2 \mu\text{m}$  (Fig. 3): more iron was extracted by hydroxylamine hydrochloride (extraction step 2) and dithionite (extraction step 3). This means that more iron is bound in the form of (oxyhydr)oxides or equivalents. Similar enrichment of the fine fractions in “oxide” Fe was observed previously in the meltwater sediments (Poulton and Raiswell, 2005) and in soils from a chronosequence in front of an Alpine glacier (Kiczka *et al.*, 2011).

In the forefield of Werenskioldbreen, the amount of oxide iron speciation (steps 2–4) increases with increasing distance from the glacier front and is the highest in samples F and M (Figs 2, 3). This evidences the higher proportion of secondary minerals in older soils and is reflected in (elec-

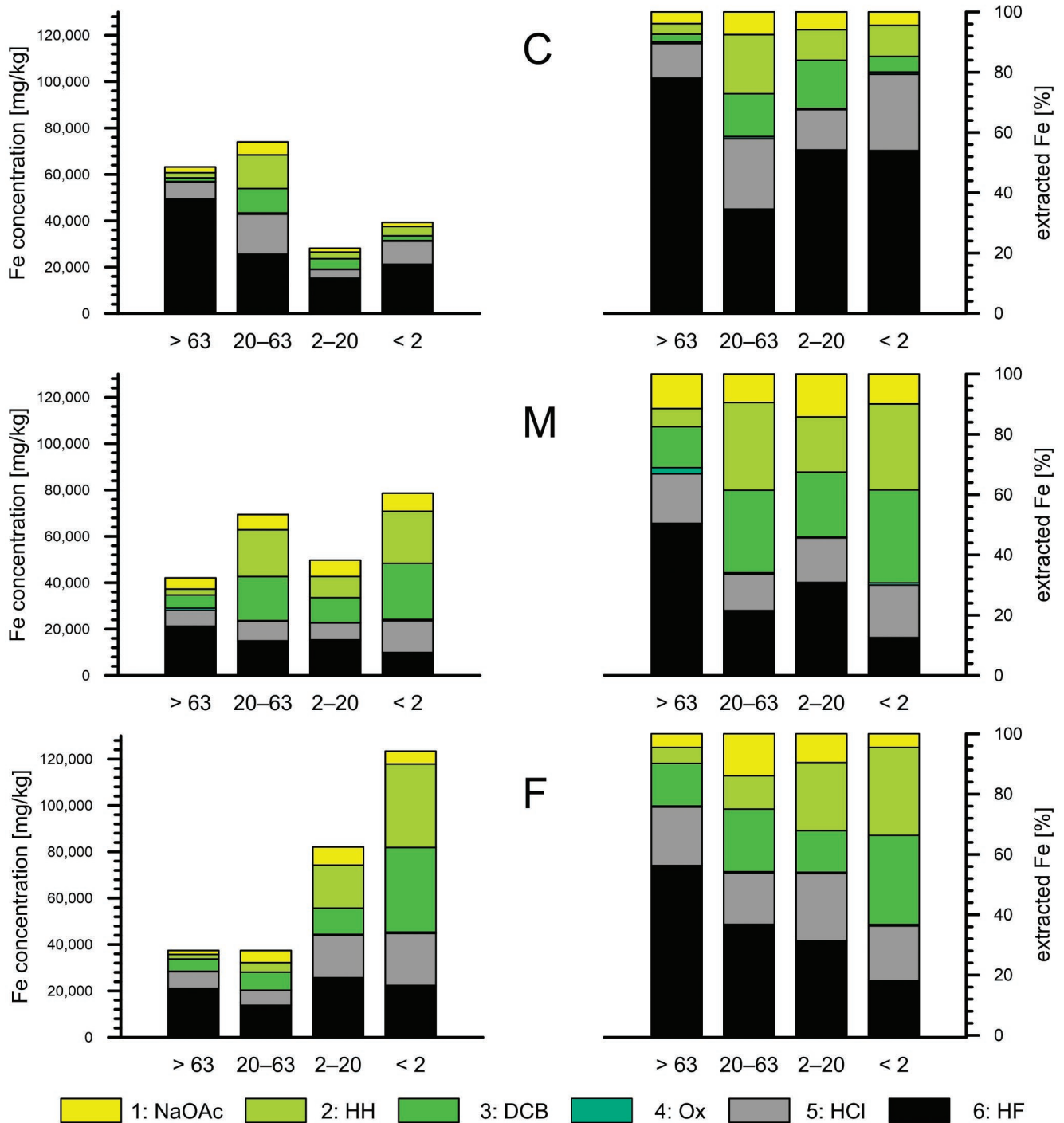


**Fig. 2.** Iron speciation in the Werenskioldbreen forefield regoliths located in close (C), middle (M) and far (F) distance from the glacier terminus, based on the results of sequential chemical extraction. Grain fractions (in  $\mu\text{m}$ ) are on the horizontal axis. The plots on the left show absolute Fe concentrations, the plots on the right show percentage proportions of individual Fe speciations.

tron) microscopic observations. SEM analysis of samples from location C reveals that iron (oxyhydr)oxides are rare and occur usually as scattered particles. In samples M and F, however, they are much more common, more morphologically diverse and often form accumulations and crusts on primary minerals (Fig. 4A–H).

An analogous tendency of increase of “reactive” iron (i.e., dissolved in oxalate buffer and in dithionite) was observed previously in soil samples (not size-separated) from

the Werenskioldbreen forefield by Kabała and Zapart (2009, 2012). In the samples of the present authors, however, the ratio of “amorphous” Fe (step 2) to “free” Fe (step 2 + 3) increases distinctly only in the 2–20  $\mu\text{m}$  fraction. The ratio decreases in other grain size fractions (Table 2). This is not in accordance to the results of Kabała and Zapart (2012). A possible explanation of this discrepancy might arise from the extraction procedures – in this work the authors carried out sequential extraction, in which the steps that extract iron

Table 1

The results of sequential chemical extraction expressed as absolute concentrations of individual speciations of the elements; b.l.d. – below limit of detection

	Fe	Mn	Cu	Pb	Zn		Fe	Mn	Cu	Pb	Zn
<b>&gt; 63 <math>\mu\text{m}</math></b>						<b>2–20 <math>\mu\text{m}</math></b>					
<b>Extraction step 1 (NaOAc): <math>\text{CH}_3\text{COONa} + \text{CH}_3\text{COOH}</math>, pH 4.5, 50°C</b>											
C	2,458	207.71	7.09	13.18	2.55	C	1,663	30.77	3.10	21.23	3.95
M	4,821	188.23	2.00	8.49	3.20	M	7,074	229.66	8.09	12.18	32.45
F	1,688	13.04	3.25	18.64	9.64	F	7,794	489.32	12.95	23.54	24.84
<b>Extraction step 2 (HH): <math>\text{HONH}_2 \cdot \text{HCl} + \text{CH}_3\text{COOH}</math></b>											
C	2,212	25.96	8.89	9.24	7.34	C	2,845	19.48	7.14	11.49	11.44
M	2,533	34.26	5.59	28.56	6.14	M	9,109	56.32	31.37	30.01	21.67
F	1,974	27.34	4.05	28.98	6.25	F	18,560	83.97	14.99	38.83	27.49
<b>Extraction step 3 (DCB): <math>\text{Na}_2\text{S}_2\text{O}_4 + \text{CH}_3\text{COOH} + \text{C}_3\text{H}_4(\text{OH})(\text{COONa})_3</math>, pH 4.8</b>											
C	1,567	6.49	3.06	3.06	17.48	C	4,488	10.05	0.62	2.87	16.61
M	5,720	29.70	b.l.d.	b.l.d.	17.54	M	10,718	38.25	b.l.d.	b.l.d.	18.60
F	5,296	24.80	1.37	b.l.d.	19.05	F	11,307	68.60	2.37	b.l.d.	16.62
<b>Extraction step 4 (Ox): <math>(\text{COONH}_4)_2 + (\text{COOH})_2</math>, pH 3.0</b>											
C	380	1.25	2.43	11.55	1.31	C	120	b.l.d.	4.68	15.05	4.37
M	844	0.69	3.18	b.l.d.	1.56	M	134	0.12	8.36	23.71	3.06
F	132	0.31	3.62	5.93	1.81	F	280	0.37	12.50	7.12	5.06
<b>Extraction step 5 (HCl): conc. HCl</b>											
C	7,251	40.01	6.68	10.11	15.80	C	3,770	21.73	2.25	9.80	8.30
M	6,938	40.84	0.69	2.81	9.92	M	7,359	38.63	1.31	2.43	12.48
F	7,270	21.55	2.06	2.19	4.56	F	18,407	65.29	4.81	1.62	10.12
<b>Extraction step 6 (HF): <math>\text{HF} + \text{HClO}_4 + \text{HNO}_3 + \text{HCl}</math>, 250°C</b>											
C	49,331	304.51	12.16	b.l.d.	94.44	C	15,246	94.35	11.36	0.69	43.21
M	21,222	150.05	10.74	4.81	35.33	M	15,355	74.20	1.87	b.l.d.	31.08
F	21,076	137.48	8.49	b.l.d.	40.35	F	25,694	81.54	3.50	b.l.d.	39.67
<b>total</b>											
C	63,198	585.93	40.31	47.14	138.91	C	28,132	176.38	29.16	61.13	87.88
M	42,078	443.77	22.20	44.67	73.69	M	49,749	437.19	51.00	68.34	119.34
F	37,437	224.52	22.85	55.74	81.67	F	82,041	789.09	51.12	71.12	123.80
<b>20–63 <math>\mu\text{m}</math></b>						<b>&lt; 2 <math>\mu\text{m}</math></b>					
<b>Extraction step 1 (NaOAc): <math>\text{CH}_3\text{COONa} + \text{CH}_3\text{COOH}</math>, pH 4.5, 50°C</b>											
C	5,582	186.24	32.46	164.28	18.82	C	1,748	36.34	5.25	47.38	60.48
M	6,562	455.99	6.49	12.99	12.54	M	7,816	509.85	12.88	20.33	64.12
F	5,212	24.22	4.39	12.74	8.84	F	5,551	1188.45	79.93	47.11	505.06
<b>Extraction step 2 (HH): <math>\text{HONH}_2 \cdot \text{HCl} + \text{CH}_3\text{COOH}</math></b>											
C	14,496	68.95	30.46	56.57	38.15	C	4,054	26.44	8.45	71.29	19.19
M	20,200	88.10	28.92	28.72	40.46	M	22,417	141.55	42.10	43.64	65.62
F	4,122	40.20	5.69	31.96	10.69	F	36,009	262.97	46.16	58.75	201.33
<b>Extraction step 3 (DCB): <math>\text{Na}_2\text{S}_2\text{O}_4 + \text{CH}_3\text{COOH} + \text{C}_3\text{H}_4(\text{OH})(\text{COONa})_3</math>, pH 4.8</b>											
C	10,510	1.87	7.61	4.56	22.53	C	2,035	66.11	0.37	1.31	11.12
M	19,019	63.55	b.l.d.	b.l.d.	24.16	M	24,228	119.59	b.l.d.	1.12	23.22
F	7,779	31.71	2.06	b.l.d.	15.92	F	36,449	196.26	1.06	b.l.d.	64.25
<b>Extraction step 4 (Ox): <math>(\text{COONH}_4)_2 + (\text{COOH})_2</math>, pH 3.0</b>											
C	536	2.06	16.85	15.10	4.37	C	277	b.l.d.	4.00	17.12	3.69
M	273	0.62	12.11	23.97	3.56	M	544	1.87	20.66	19.97	3.31
F	132	0.31	4.43	6.62	2.18	F	599	2.19	41.53	6.74	5.31
<b>Extraction step 5 (HCl): HCl</b>											
C	17,282	70.40	9.80	12.80	31.08	C	9,976	41.86	4.12	8.00	16.99
M	8,426	40.08	2.00	2.18	7.62	M	13,727	63.55	8.30	2.31	20.47
F	6,417	25.84	1.31	1.25	3.50	F	22,466	80.74	6.24	2.19	11.12
<b>Extraction step 6 (HF): <math>\text{HF} + \text{HClO}_4 + \text{HNO}_3 + \text{HCl}</math>, 250°C</b>											
C	25,579	151.17	8.99	4.06	74.96	C	21,217	120.27	5.56	b.l.d.	51.92
M	14,945	82.16	2.43	b.l.d.	37.33	M	9,878	64.11	2.12	b.l.d.	39.02
F	13,767	93.51	13.92	b.l.d.	29.46	F	22,321	60.26	1.75	b.l.d.	25.23
<b>total</b>											
C	73,986	480.70	106.17	257.36	189.92	C	39,307	291.01	27.75	145.10	163.39
M	69,425	730.51	51.95	67.86	125.66	M	78,609	900.52	86.07	87.38	215.77
F	37,429	215.79	31.81	52.56	70.59	F	123,393	1790.87	176.67	114.79	812.29

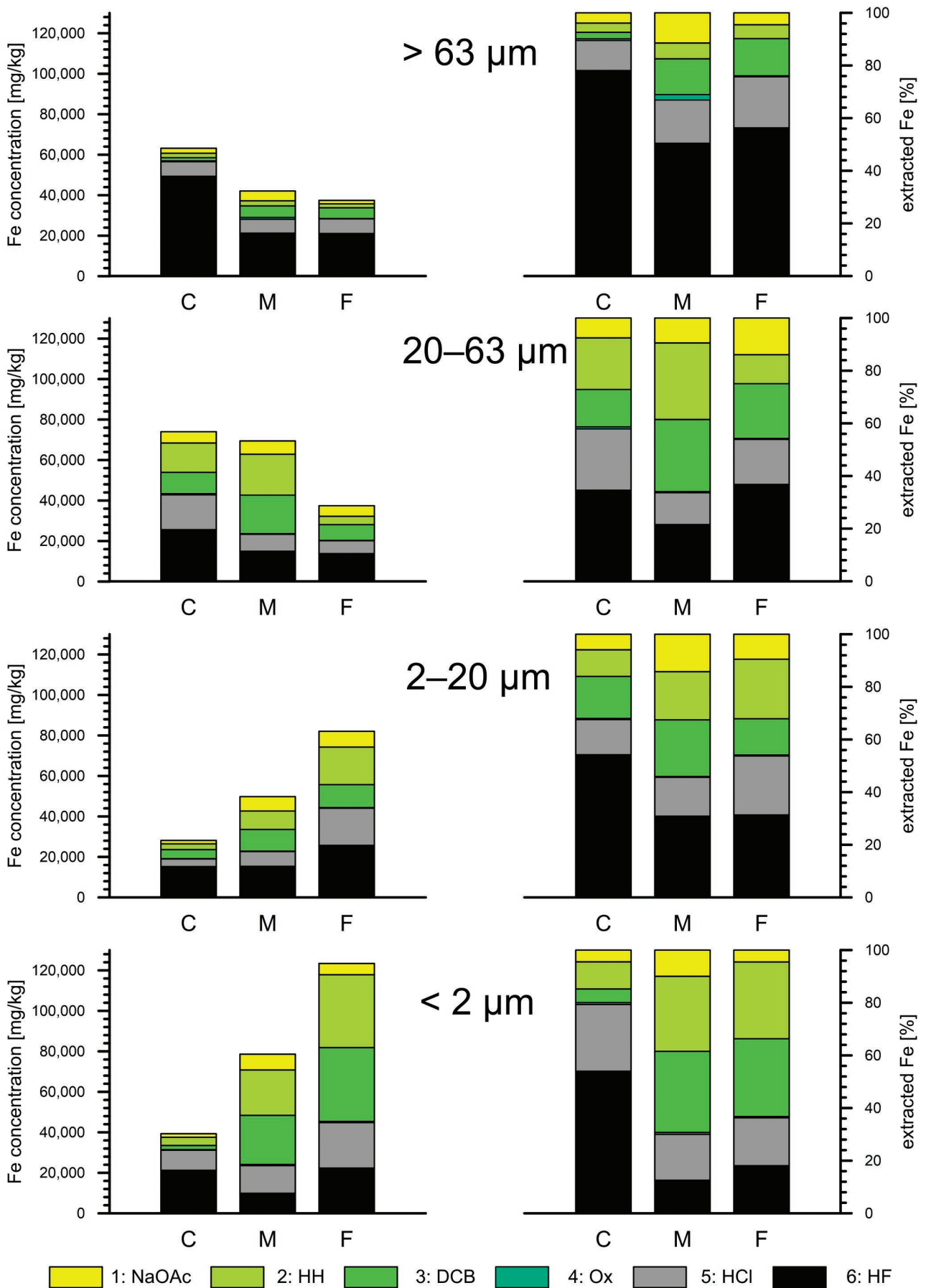


**Fig. 3.** Iron speciation in various grain fractions of the Werenskioldbreen forefield regoliths. The plots on the left show absolute Fe concentrations, the plots on the right show percentage proportions of individual Fe speciations. The letters at the horizontal axes denote sample locations in the chronosequence.

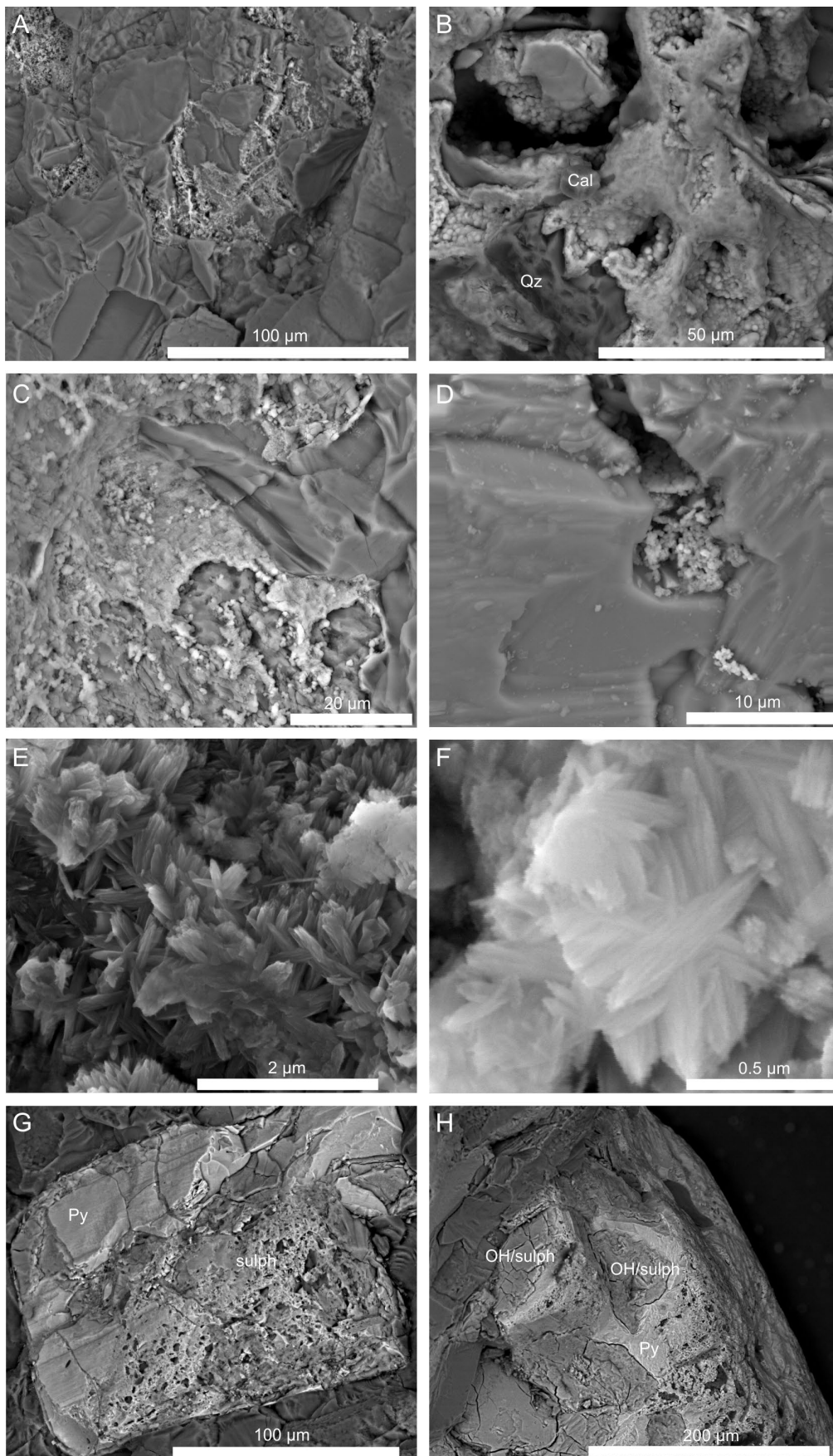


**Fig. 4.** Back-scattered electron images of iron minerals. **A.** Accumulations of iron oxyhydroxide (bright) filling voids within quartz crystals in sample F. **B.** Accumulations of iron oxyhydroxide in sample M; Qz – quartz, Cal – calcite. **C.** Discontinuous iron oxyhydroxide crust on the surface of calcite in sample F. **D.** Iron oxyhydroxide (probably ferrihydrite) filling a void within large dolomite crystal in sample M. **E.** Goethite accumulation in sample F. **F.** Elongated goethite crystals in sample F. **G.** An early stage of pyrite (Py) weathering to iron sulphate (sulph) in sample M. **H.** iron oxyhydroxide/sulphate crust (OH/sulph) on weathered pyrite (Py) in sample M.

**Table 2**

The proportions of “amorphous”, “free”, and total Fe concentrations in the samples;  $Fe_{HH}$  – hydroxylamine hydrochloride-extracted iron (i.e., bound in ferrihydrite and other “amorphous” oxyhydroxides),  $Fe_{DCB}$  – dithionite-citrate-bicarbonate-extracted iron (i.e., bound in all oxide-oxyhydroxide phases except for magnetite; the sum of Fe extracted in steps 2 and 3),  $Fe_T$  – total extracted iron (the sum of Fe extracted in all steps)

	$Fe_{HH}/Fe_{DCB}$	$Fe_{DCB}/Fe_T$		$Fe_{HH}/Fe_{DCB}$	$Fe_{DCB}/Fe_T$
<b>&gt; 63 <math>\mu\text{m}</math></b>			<b>2–20 <math>\mu\text{m}</math></b>		
<b>C</b>	0.59	0.06	<b>C</b>	0.39	0.20
<b>M</b>	0.31	0.20	<b>M</b>	0.46	0.40
<b>F</b>	0.27	0.19	<b>F</b>	0.62	0.36
<b>20–63 <math>\mu\text{m}</math></b>			<b>&lt; 2 <math>\mu\text{m}</math></b>		
<b>C</b>	0.58	0.64	<b>C</b>	0.67	0.15
<b>M</b>	0.52	0.56	<b>M</b>	0.48	0.59
<b>F</b>	0.35	0.32	<b>F</b>	0.50	0.59

oxide phases were preceded by carbonate dissolution. In the work of Kabała and Zapart (2012), the oxalate treatment led to the dissolution of other labile species of iron. In this paper, the authors point that “acid oxalate-extractable Fe is a measure of most reactive forms, e.g., water-soluble, exchangeable, poorly crystalline or short-range ordered, and a fraction of organically-bound Fe”. Moreover, they observed an increase of “oxalate” to “dithionite” iron ratio only in the surface soil horizons (0–3 cm). If correct, the results of the present study might suggest that initially formed ferrihydrite is quickly transformed into more stable “crystalline” (oxyhydr)oxides, like goethite.

The ratio of oxide (“free”) to total iron ranges in the Werenskioldbreen forefield from 0.06 to 0.6. The lowest content is observed in the coarsest fraction (> 63  $\mu\text{m}$ ) of sample C (Table 2). The ratio is distinctly higher in samples M and F, with the exception of the 20–63  $\mu\text{m}$  fraction. This again indicates a higher proportion of weathering products in older soils. In samples M and F, an increase in  $Fe_{DCB}/Fe_T$  ratios (a ratio of iron oxides to total iron) with decreasing grain size is apparent and the trend is not readable in sample C (Table 2). At the same time, the virtually identical  $Fe_{DCB}/Fe_T$  ratios in the corresponding fractions of samples M and F can be related to the nonlinear weathering in a glacier forefield (Righi *et al.*, 1999; He and Tang, 2008; Mavris *et al.*, 2010). This can slow down with time in the case of Arctic glaciers (Dahms *et al.*, 2012), mainly owing to the plant succession, which is limited by water availability (Kabała and Zapart, 2012). The oxidation of sulphides and hence the release of reactive iron could be hampered by the formation of weathering crusts on the surfaces of primary minerals, which can be an important feature in older soils (Szynkiewicz *et al.*, 2013). Secondary crusts were observed with SEM on the grains of primary minerals in samples M and F (Fig. 4G–H; see also fig. 7 in Kwaśniak-Kominek *et al.*, 2016).

Although the authors were not able to identify unambiguously secondary iron minerals, on the basis of SEM imaging they suspect the occurrence of mainly ferrihydrite and

goethite and maybe also of schwertmannite. The nanoparticles of these phases have been encountered previously in glacial sediments and glacial meltwaters in the polar regions (Raiswell *et al.*, 2008, 2009; Raiswell, 2011a; Hawking *et al.*, 2014). Very low solubility products, especially of ferrihydrite ( $10^{-38.5}$  for 2-L ferrihydrite and  $10^{-39.5}$  for 6-L ferrihydrite; Hiemstra, 2015) and goethite ( $< 10^{-40}$ ; Cornell and Schwertmann, 2003), in combination with the slightly alkaline pH of the pore water, favour their formation and stability. The results of hydrogeochemical modelling showed that the pore water in the soils studied are oversaturated with respect to goethite and microscopic observations revealed the occurrence of goethite rims on the surfaces of several grains of pyrite (Kwaśniak-Kominek *et al.*, 2016). Goethite was also identified as a dominant oxide-type Fe carrier in the soils of the Hornsund area (Szymański *et al.*, 2015; Gonet *et al.*, 2018). The accumulations of elongated goethite crystallites on grain surfaces in the “older” samples were relatively common in SEM micrographs (Fig. 4E–F). The aggregates of cryptocrystalline iron (oxyhydr)oxides, probably ferrihydrite, were locally quite frequent as well (Fig. 4B, D). The spheroidal shape and the dimensions of the aggregates suggest a possible microbial origin of the ferrihydrite. Moreover, iron (oxyhydr)oxides in sample F often were encountered in cracks and voids in the rock fragments, suggesting that their dissolution is responsible for iron leached by hydroxylamine hydrochloride and dithionite from the coarser fractions (20–63  $\mu\text{m}$  and > 63  $\mu\text{m}$ ).

The relatively high pH of pore water does not favour the formation of schwertmannite, which precipitates from acidic solutions (Bigham *et al.*, 1996; Regenspurg *et al.*, 2004; Zhang *et al.*, 2018). Its formation is possible, however, in the specific microenvironments arising around oxidizing pyrite grains. Intensive pyrite weathering in the area is indicated by analyses of shallow groundwaters and surface waters in the forefield of the Werenskioldbreen Glacier (Olichwer *et al.*, 2013; Kwaśniak-Kominek *et al.*, 2016; Stachnik *et al.*, 2016). Szynkiewicz *et al.* (2013) found, on the basis of sulphur isotope ratios, that sulphate ions in the waters of this area originate mainly from the weathering of sulphides present in quartz and carbonate veins. Abundant evidence of the chemical alteration of pyrite grains was found by SEM imaging and these processes appear to be more common in the samples, collected at a distance from the glacier terminus (Fig. 4G–H). An indirect result of these processes is a decrease of pore water pH – from 8.57 in the youngest soil, to 7.22 in the oldest, even though the decrease also is related to carbonate leaching (Kwaśniak-Kominek *et al.*, 2016). Similar results were obtained by Kabała and Zapart (2009), who pointed out, however, the role of acidic humic matter originating from the more enhanced vegetation in older soils. The contribution of vegetation in lowering the pH of the soils is of minor importance. Mapelli *et al.* (2018), who studied soil chronosequence on the forefield of Midtre Lovénbreen glacier, reported a decrease of rhizospheric pH from 8.17 down to 6.17 only in soil matured for over 1,900 years, whereas the pH of barren and developing soils did not change significantly. Also, the concentration of organic acids in soils, influenced by plant roots, was not found to increase substantially for the first hundred years of soil

development (Mapelli *et al.*, 2018). Organic carbon concentrations in the Werenskioldbreen forefield is rather low, compared with an increasing gradient along the chronosequence (Kabała and Zapart, 2012; Stachnik *et al.*, 2016).

Despite the conditions that do not exclude schwertmannite precipitation, the mineral is probably not a significant iron carrier in the soils studied. Calculations by Raiswell *et al.* (2009) indicated that the life span of schwertmannite in the contact with cold (0 °C) water at neutral pH is about one to two years, with goethite and/or ferrihydrite being the transformation products.

A few to a dozen or so percent of the total iron was extracted from the samples by acetate buffer (step 1), suggesting Fe bonding in carbonates and equivalent forms (Figs 1, 2). This is consistent with the results of previous works, which reported high carbonate concentrations, particularly in the younger soils (Kabała and Zapart, 2009, 2012). Moreover, Kowalska and Sroka (2008) found 23–38% of marbles and marble-quartzite conglomerates within pebbles in the Werenskioldbreen forefield. Taking into account the geology of the area, the most probable carbonate iron carriers are siderite and/or ferrous dolomite (ankerite) (Czerny *et al.*, 1992b; Figura *et al.*, 2014). Distinctly higher proportions of acetate-extracted iron were found in the older soils, particularly in the M sample (Table 3), which might be partly an effect of the presence of “exchangeable” species. Previous mineralogical analyses of samples, collected from the outcrops in the vicinity of Werenskioldbreen and in the glacier forefield, revealed that siderite already is partly weathered before it enters the regolith, with goethite, lepidocrocite and hematite as the weathering products (Figura *et al.*, 2014).

A descending trend of the HCl- and HF-extracted Fe (extraction steps 5 and 6) in the coarser-grained fractions at a distance from the glacier front indicates that the content of primary minerals decreases in the older soils (Fig. 3). In the > 63 µm fraction, these species contribute approximately 90% of the total iron content in sample C while only ca. 75% in sample F. Despite the fact that in the fines of older soils the proportion of silicate species decreases, the total amount of the species increases. For example, a sum of HCl- and HF-extracted Fe concentrations in the < 2 µm fraction of sample C amounts to ca. 3.1 wt.%, whereas in sample F it is as high as 4.5 wt.% (Table 1).

### Manganese

Manganese occurs in much lower concentrations than iron (Fig. 5). The total Mn content ranges from 225 ppm to 586 ppm in the fraction > 63 µm and increases in the finest fraction (< 2 µm) to 291–1791 ppm (Table 1; Fig. 6). The trend is consistent with the manganese content in soil of the Russian Arctic (Moskovchenko *et al.*, 2017). Comparable values were obtained for soils from Bellsund (Melke, 2006; Melke and Chodorowski, 2006) and Kaffiøyra (Plichta and Kuczyńska, 1991). Slightly higher manganese levels in similar soils from Fugglebeken were obtained using a different methodology and therefore cannot be directly compared to the results in the present study (Szymański *et al.*, 2013). Like Fe, Mn content in the coarse-grained fraction (> 63 µm) decreases with distance from the glacial front of Werenski-

oldbreen (from 586 ppm in sample C to 225 ppm in sample F). The opposite was observed in fine fractions (Fig. 6): Mn in fraction < 2 µm increases from 291 ppm at location C to 1791 ppm at location F. Hence, Mn is concentrated in the coarse-grained material of sample C: there is two times more Mn in the fraction > 63 µm than in the fraction < 2 µm. In all other samples it is concentrated in the fine-grained material. This is particularly apparent in sample F: there is approximately eight times more Mn in the fraction < 2 µm than in the fraction > 63 µm (Fig. 6).

From the fraction > 63 µm, the large amounts of Mn were extracted mostly by strong acids: hydrofluoric and hydrochloric (extraction steps 5 and 6). These two reagents extracted up to 70% Mn (Fig. 6). Therefore, in the coarsest-grained material Mn occurs predominately in the form of silicates. The amount of silicate-bound Mn decreases two times with the increasing distance from the glacier terminus: from 345 ppm in sample C to 159 ppm in sample F (Fig. 6). The concentration of carbonate-related manganese species decreases as well, which is evidenced by the decrease in acetate-extracted Mn: 208 ppm in the youngest soil C, 188 ppm in sample M and 13 ppm in the oldest soil F (Table 1). Weathering of carbonates might be an important source of manganese in the Werenskioldbreen forefield, since both siderite and ankerite are common in the area and contain up to several wt.% of Mn (Czerny *et al.*, 1992b). This results in the formation of Mn oxide crusts observed on altered carbonates in the field.

In the fine fractions, the amount of relatively labile manganese (extraction steps 1 and 2) increases at the expense of residual manganese. The labile manganese forms amounts of up to approximately 70% of the total Mn content in the 20–63 µm and 2–20 µm fractions up to as high as ca. 80% in the fraction < 2 µm of the older soils (Fig. 6). Iron oxide-bound manganese appears to increase in the fine-grained fractions as well, which is reflected in the distinctly higher Mn levels extracted at step 3 (66–196 ppm in fraction < 2 µm compared to < 3 ppm in fraction > 63 µm). On the basis of the observed trends, it is apparent that in the youngest soil (sample C), Mn is bound mainly in primary silicates, which concentrate rather in the coarse-grained material. In the more distant soils, a gradual increase in labile and oxide-bound Mn is observed. This is consistent with SEM analyses: aggregates of cryptocrystalline manganese oxides were encountered only in samples M and F. Moreover, the presence of Mn was detected in some iron oxyhydroxides. This is also reflected in increasing Mn concentrations in the fine-grained material and in decreasing Mn concentrations in the coarse-grained material.

The behaviour of manganese in the Werenskioldbreen forefield is similar to that of iron. This is an effect of comparable mineralogy and geochemistry of these two elements. Mn isomorphically substitutes Fe in primary (alumino)silicates, as biotite, chlorite, pyroxenes and amphiboles, which are common rock-forming minerals in the area (Czerny *et al.*, 1992a, b; Kwaśniak-Kominek *et al.*, 2016). Mn and Fe coexist also in the common carbonates, predominately siderite and ankerite (Figura *et al.*, 2014). Hence, both elements are simultaneously released from primary minerals and can meet again in similar secondary phases.

Table 3

The results of sequential chemical extraction expressed as relative percentage proportions of individual speciations of the elements

	Fe	Mn	Cu	Pb	Zn		Fe	Mn	Cu	Pb	Zn
<b>&gt; 63 µm</b>						<b>2–20 µm</b>					
<b>Extraction step 1 (NaOAc): CH<sub>3</sub>COONa + CH<sub>3</sub>COOH, pH 4.5, 50°C</b>											
C	4	35	18	28	2	C	6	17	11	35	4
M	11	42	9	19	4	M	14	53	16	18	27
F	5	6	14	33	12	F	9	62	25	33	20
<b>Extraction step 2 (HH): HONH<sub>2</sub> · HCl + CH<sub>3</sub>COOH</b>											
C	4	4	22	20	5	C	10	11	24	19	13
M	6	8	25	64	8	M	18	13	62	44	18
F	5	12	18	52	8	F	23	11	29	55	22
<b>Extraction step 3 (DCB): Na<sub>2</sub>S<sub>2</sub>O<sub>4</sub> + CH<sub>3</sub>COOH + C<sub>3</sub>H<sub>4</sub>(OH)(COONa)<sub>3</sub>, pH 4.8</b>											
C	2	1	8	6	13	C	16	6	2	5	19
M	14	7	0	0	24	M	22	9	0	0	16
F	14	11	6	0	23	F	14	9	5	0	13
<b>Extraction step 4 (Ox): (COONH<sub>4</sub>)<sub>2</sub> + (COOH)<sub>2</sub>, pH 3.0</b>											
C	1	0	6	24	1	C	0	0	16	25	5
M	2	0	14	0	2	M	0	0	16	35	3
F	0	0	16	11	2	F	0	0	24	10	4
<b>Extraction step 5 (HCl): conc. HCl</b>											
C	11	7	17	21	11	C	13	12	8	16	9
M	16	9	3	6	13	M	15	9	3	4	10
F	19	10	9	4	6	F	22	8	9	2	8
<b>Extraction step 6 (HF): HF + HClO<sub>4</sub> + HNO<sub>3</sub> + HCl, 250°C</b>											
C	78	52	30	0	68	C	54	53	39	1	49
M	50	34	48	11	48	M	31	17	4	0	26
F	56	61	37	0	49	F	31	10	7	0	32
<b>20–63 µm</b>						<b>&lt; 2 µm</b>					
<b>Extraction step 1 (NaOAc): CH<sub>3</sub>COONa + CH<sub>3</sub>COOH, pH 4.5, 50°C</b>											
C	8	39	31	64	10	C	4	12	19	33	37
M	9	62	12	19	10	M	10	57	15	23	30
F	14	11	14	24	13	F	4	66	45	41	62
<b>Extraction step 2 (HH): HONH<sub>2</sub> · HCl + CH<sub>3</sub>COOH</b>											
C	20	14	29	22	20	C	10	9	30	49	12
M	29	12	56	42	32	M	29	16	49	50	30
F	11	19	18	61	15	F	29	15	26	51	25
<b>Extraction step 3 (DCB): Na<sub>2</sub>S<sub>2</sub>O<sub>4</sub> + CH<sub>3</sub>COOH + C<sub>3</sub>H<sub>4</sub>(OH)(COONa)<sub>3</sub>, pH 4.8</b>											
C	14	0	7	2	12	C	5	23	1	1	7
M	27	9	0	0	19	M	31	13	0	1	11
F	21	15	6	0	23	F	30	11	1	0	8
<b>Extraction step 4 (Ox): (COONH<sub>4</sub>)<sub>2</sub> + (COOH)<sub>2</sub>, pH 3.0</b>											
C	1	0	16	6	2	C	1	0	14	12	2
M	0	0	23	35	3	M	1	0	24	23	2
F	0	0	14	13	3	F	0	0	24	6	1
<b>Extraction step 5 (HCl): HCl</b>											
C	23	15	9	5	16	C	25	14	15	6	10
M	12	5	4	3	6	M	17	7	10	3	9
F	17	12	4	2	5	F	18	5	4	2	1
<b>Extraction step 6 (HF): HF + HClO<sub>4</sub> + HNO<sub>3</sub> + HCl, 250°C</b>											
C	35	31	8	2	39	C	54	41	20	0	32
M	22	11	5	0	30	M	13	7	2	0	18
F	37	43	44	0	42	F	18	3	1	0	3

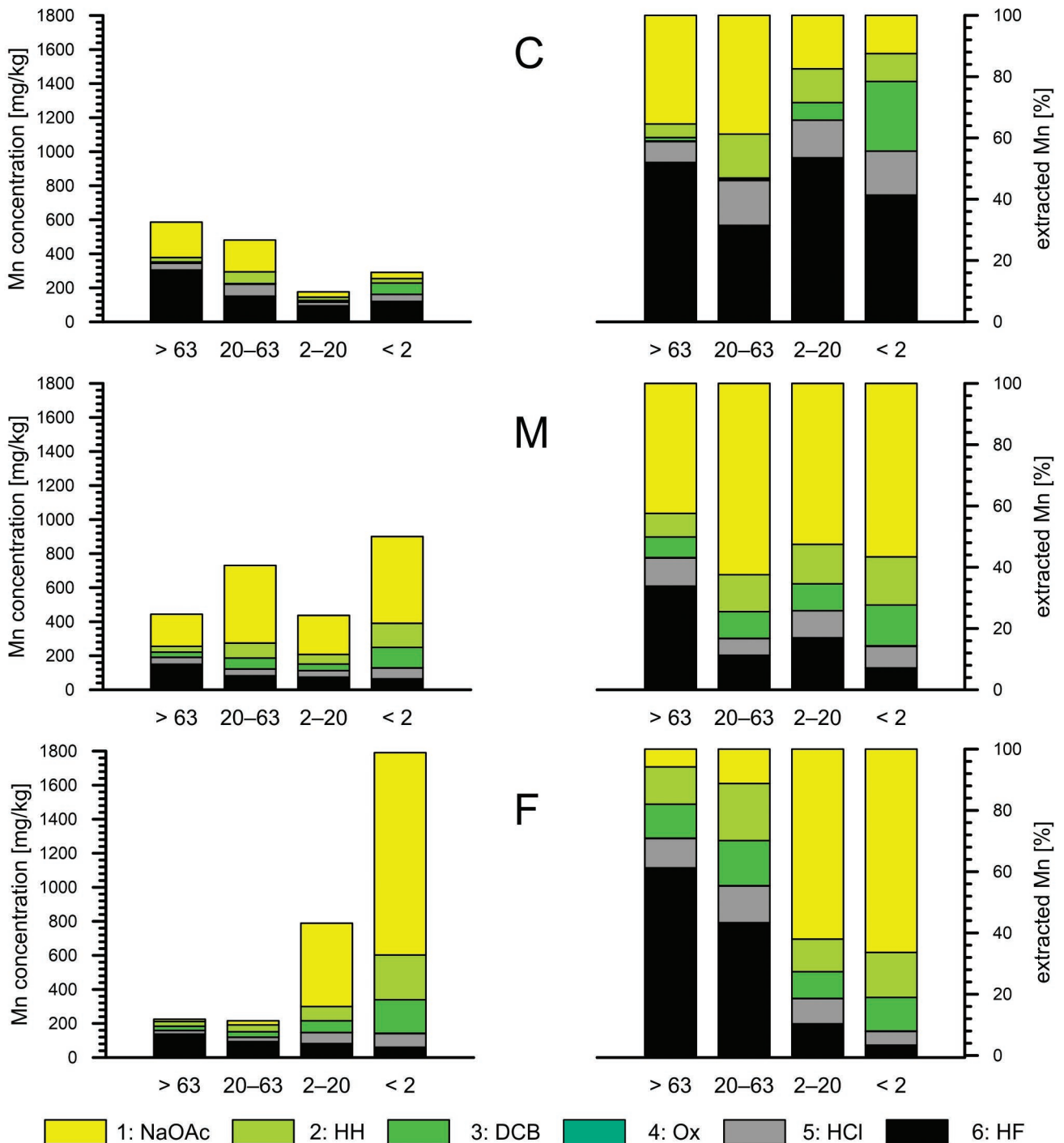


Fig. 5. Manganese speciation in the Werenskioldbreen chronosequence. See Figure 2 for explanations.

### Copper

Copper concentrations are low at all locations (Fig. 7). Its total content in fraction > 63 μm ranges from 22 ppm to 40 ppm and increases slightly in the finer fractions up to 27–177 ppm in the fraction < 2 μm (Table 1). Similar levels were reported in the Arctic (Melke and Chorodowski, 2006; Plichta and Kuczyńska, 1991; Krajcarová *et al.*, 2016; Zaborska *et al.*, 2017) and in Antarctica (Fabri-Jr *et al.*, 2018). Much lower content was found by

Gonet *et al.* (2018) at unpolluted sites in the Hornsund area and by Moskovchenko *et al.* (2017) in various soils of the Russian Arctic. The content of Cu in coarse-grained fractions (i.e., > 63 μm and 20–63 μm) decreases with increasing distance from the glacier terminus but it increases distinctly in fine fractions (i.e., 2–20 μm and < 2 μm). In sample C, there is 1.5 times more Cu in the fraction > 63 μm, compared to < 2 μm (Fig. 8). On the contrary, the copper contents in the finest fraction (< 2 μm) of samples M and F are four to even eight times higher than in the

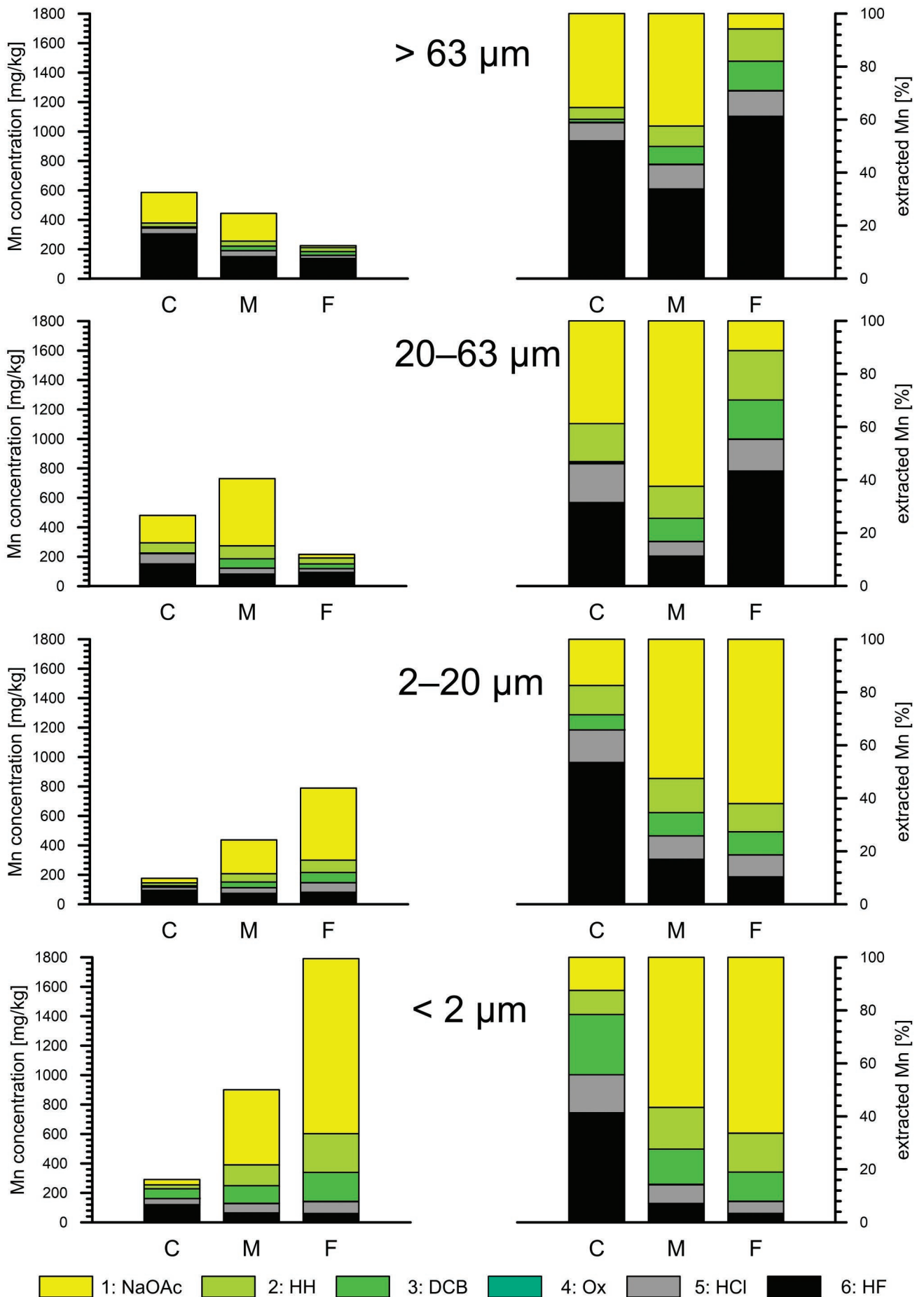


Fig. 6. Manganese speciation in various grain fractions of the Werenskioldbreen chronosequence. See Figure 3 for explanations.

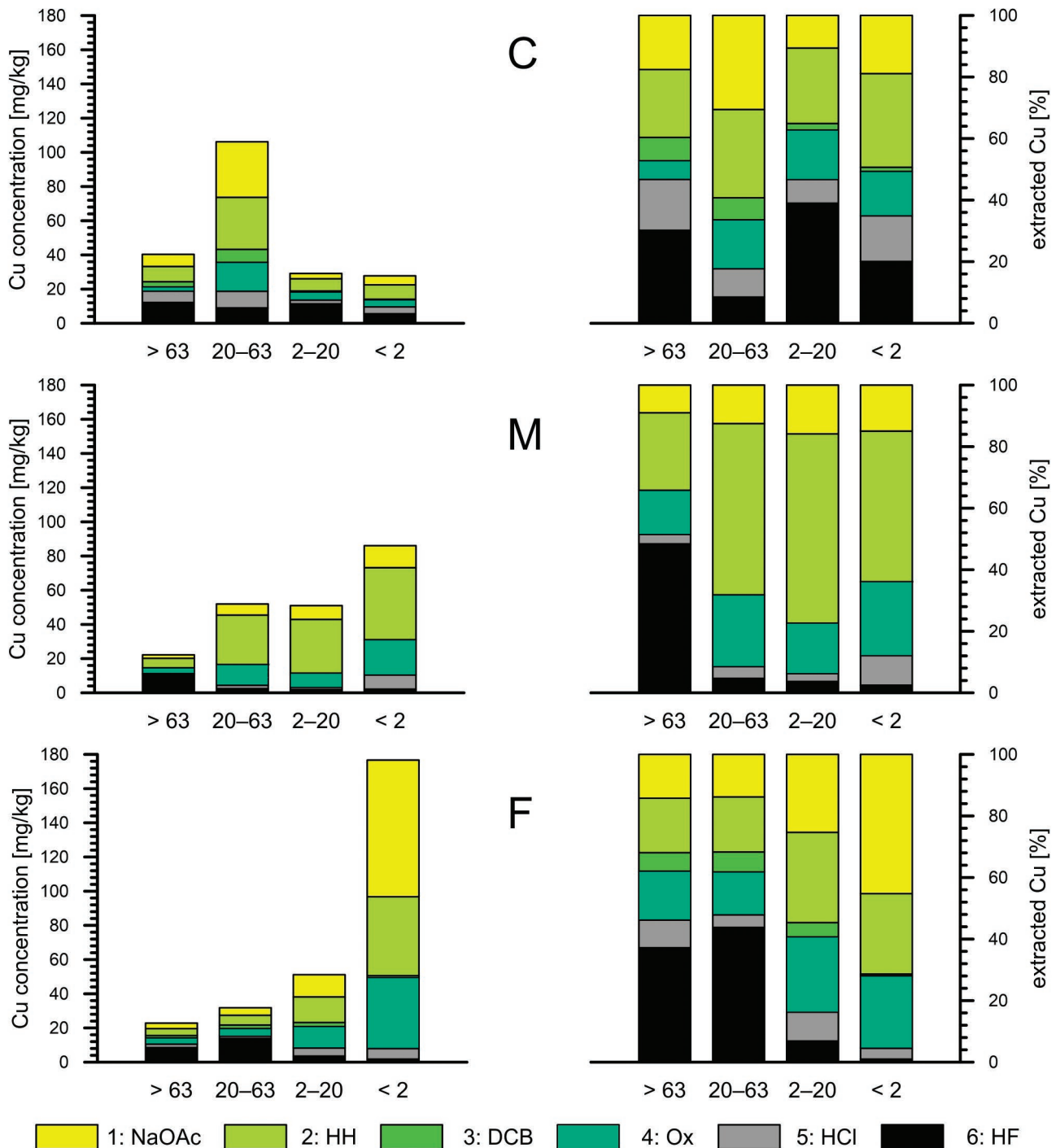


Fig. 7. Copper speciation in the Werenskioldbreen chronosequence. See Figure 2 for explanations.

coarsest (> 63  $\mu\text{m}$ ) fraction (Table 1). This is consistent with Melke's observation (2006) that bioavailable copper in Bellsund soils is correlated with the fine fraction in the soil.

Copper speciation in different grain fractions and at different distances from the glacier front is discernible as well (Figs 7, 8). In the fraction > 63  $\mu\text{m}$ , high Cu levels (up to approximately 50% of the total amount) were not extracted until the last two steps (5 and 6, strong acids). In the finer fractions, these extractions are less important and the more labile forms, extracted in the first two or three steps, predominate (Tables 1, 3). In 20–63  $\mu\text{m}$  fraction, a decrease

in Cu content with increasing soil age is apparent (Fig. 8). Moreover, copper from this material was extracted mainly from exchangeable and carbonate species (extraction step 1) and oxide species (steps 2–4). On the other hand, an increase in the proportion of silicate forms in sample F is rather surprising and was not yet explained (Table 3).

A significant increase in copper content (several times) with the distance from the glacier terminus is observed for the finest fraction < 2  $\mu\text{m}$  (Fig. 8). This is probably an effect of chemical and physical weathering alterations, which favoured the accumulation of fine-crystalline minerals pref-

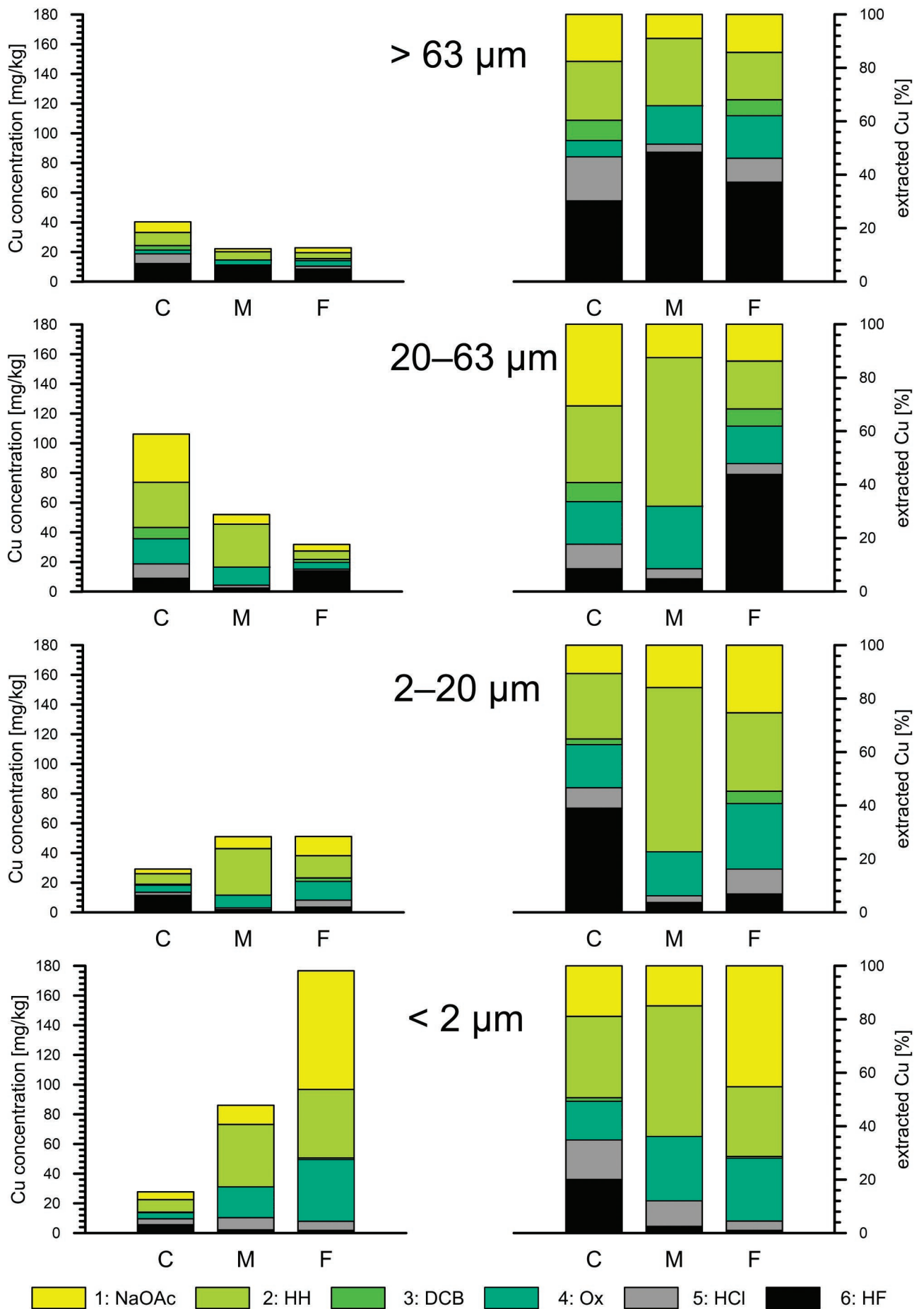


Fig. 8. Copper speciation in various grain fractions of the Werenskioldbreen chronosequence. See Figure 3 for explanations.

entially binding this element. The role of silicate species in the finest grain fractions (2–20  $\mu\text{m}$  and  $< 2 \mu\text{m}$ ) declines, with the exception of the relatively fresh sample C. A much more important role is played by forms dissolved in acetate buffer (i.e., carbonate-bound) and hydroxylamine hydrochloride (i.e., “easily reducible” Fe and Mn oxides). A proportion of Cu higher than for other elements and grain fractions was extracted in oxalate (i.e., potentially spinel-bound fraction) and is also noteworthy. The “carbonate” and “spinel” fraction contents appear to increase with the soil age, whereas the “oxide” fraction seems to be independent of the soil age.

### Lead

The lead contents in all the samples studied are low. In the coarse fraction  $> 63 \mu\text{m}$ , the concentrations are on approximately the same level at all three locations, ranging from 45 ppm to 56 ppm (Fig. 9). They are higher in the finer fractions, ranging from 87 ppm up to 145 ppm in the fraction  $< 2 \mu\text{m}$  (Table 1). In Bellsund and unpolluted Hornsund soils, Pb concentrations of up to approximately 50 ppm were reported (Melke and Chodorowski, 2006; Gonet *et al.*, 2018), whereas those detected in Kaffiøyra and Pyramiden soils did not exceed 25 ppm and 37 ppm, respectively

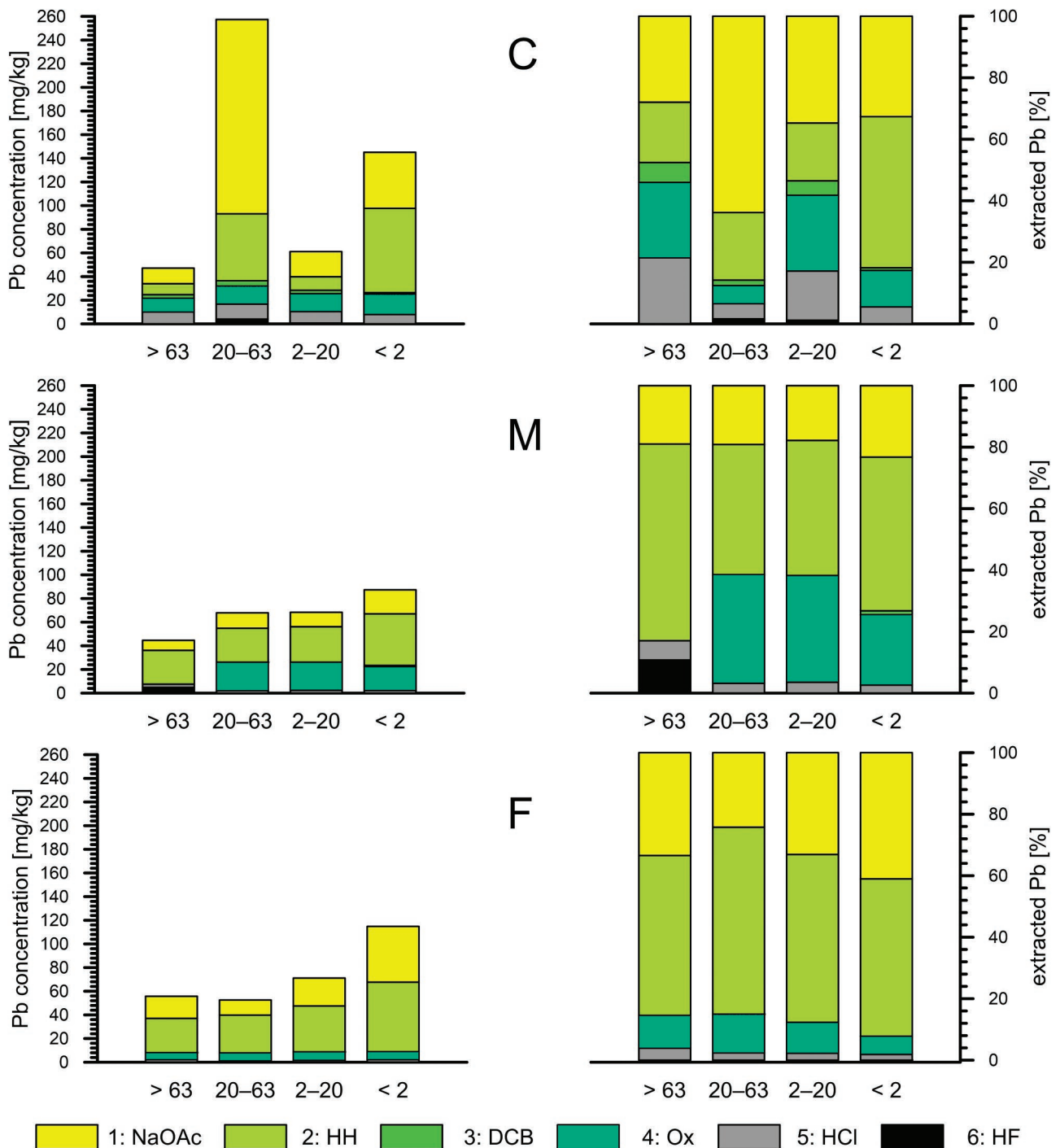


Fig. 9. Lead speciation in the Werenskioldbreen chronosequence. See Figure 2 for explanations.

(Plichta and Kuczyńska, 1991; Krajcarová *et al.*, 2016). In gelic gleysols and gelic histosols of Belyi Island, concentrations of up to 132 ppm were noted (Moskovchenko *et al.*, 2017). In sediment cores collected from several Svalbard fjords Pb concentrations ranged from ca. 6 to ca. 46 ppm (Zaborska *et al.*, 2017).

In all the soils, an increase of lead content with decreasing grain size was observed – from 47 ppm to 145 ppm in sample C, from 45 ppm to 87 ppm in sample M, and from 56 ppm up to 177 ppm in sample F. The sole exception from this trend is high Pb level in the fraction 20–63  $\mu\text{m}$  of sample C (Fig. 9).

Lead speciation is the most diversified in the sample located closest to the glacier terminus. Here, a relatively high amount of lead is associated with silicates in all grain fractions (Figs 9, 10). In older soils, the growing importance of hydroxylamine hydrochloride-extracted Pb (extraction step 2) is noteworthy. The older soils also reveal a distinctly higher proportion of carbonate-bound Pb (i.e., extractable in acetate buffer; step 1) in the finest-grained fraction (< 2  $\mu\text{m}$ ). Lead extractable in 1–4 steps, i.e., exchangeable, carbonate and (oxyhydr)oxide speciations, constitute – depending on the grain size – from 78 to 95% of the total Pb in sample C, from 83 to 97% in sample M, and from 96 up to 98% in sample F (Table 3). These forms tend to gain importance with increasing soil age and decreasing grain size.

### Zinc

Compared to the other trace elements, zinc concentrations in the soils studied are relatively high, but variable (Figs 11, 12). In the fraction > 63  $\mu\text{m}$ , the total zinc content ranges from 74 ppm in sample M up to 139 ppm in sample C. In the fraction < 2  $\mu\text{m}$ , the Zn content rises significantly and ranges from 163 ppm in sample C to as high as 812 ppm in sample F (Table 1). Diversified Zn concentrations, ranging from ca. 40 ppm up to ca. 150 ppm, were found in soils from Chamberlaindalen by Melke and Chodorowski (2006). Plichta and Kuczyńska (1991), Krajcarová *et al.* (2016), as well as Moskovchenko *et al.* (2017), and Fabri *et al.* (2018) report similar results. Much lower values were detected by Gonet *et al.* (2018) in unpolluted Hornsund soils.

With an increase in distance from the glacier front, a decrease in the total zinc content in coarser grain fractions was observed (Fig. 12): from 139 ppm in sample C to 82 ppm in sample F in the case of the fraction > 63  $\mu\text{m}$  and from 190 ppm in sample C to 71 ppm in sample F in the case of the fraction 20–63  $\mu\text{m}$  (Table 1). Conversely, the zinc content in the finer fractions appears to increase at the same time (Fig. 12): from 88 ppm in sample C up to 124 ppm in sample F in the case of the fraction 2–20  $\mu\text{m}$  and from 163 ppm up to 812 ppm in the case of the fraction < 2  $\mu\text{m}$ , respectively.

In the coarsest-grained fractions (> 63  $\mu\text{m}$ ), zinc is concentrated predominately in residuum (35–94% of the total concentrations), which means that the major Zn-bearing minerals, particularly in sample C, are silicates and (probably) sulphides (Table 3). The percentage proportion of (oxyhydr)oxide species (i.e., leached by hydroxylamine hydrochloride and dithionite; extraction steps 2 and 3) is

increasing from ca. 18% up to ca. 30% with the increasing distance from the glacier terminus, although the absolute concentrations of oxide-bound Zn remain approximately constant. A similar trend is observed in the fraction 20–63  $\mu\text{m}$  (Table 3).

The opposite trends are observed in the fine-grained material. In the case of 2–20  $\mu\text{m}$  fraction, zinc concentrations increase from 88 ppm to 124 ppm with increasing distance from the glacier front (Table 1). The percentage proportions of carbonate species (i.e., extracted at the first step) increase as well. Although absolute concentrations of Zn bound in silicates are constant with the soil age, their percentage proportions decrease from nearly 60% in sample C down to ca. 36–40% in samples M and F (Fig. 12). Similar trends can be observed in the finest grain separates (< 2  $\mu\text{m}$ ), though a fourfold increase in a total Zn concentration in sample F (to 800 ppm) is a significant feature. The latter results from high contents of zinc in carbonate and (oxyhydr)oxide forms. In the other samples, the total Zn concentrations in the fraction < 2  $\mu\text{m}$  oscillate around 200 ppm, being much higher than those in the coarser fractions. The percentage proportions of silicate speciations (extraction steps 5 and 6) in the finest fraction drop from 42% in sample C to as low as 4% in sample F.

### DISCUSSION

All the results presented above indicate that the weathering in the proglacial area of Werenskiold Glacier is very fast. In only 70–80 years, the primary mineral carriers of Fe, Mn, Pb, Zn, and Cu are to a large extent altered into secondary mineral species and ionic constituents transported away in solution or sorbed onto the initial soil skeleton. These processes are most intense close to the glacier terminus in freshly exposed sediment. Very few regional geological processes are so rapid, meaning fast enough to be comparable to rates of climate change.

The very high rate of weathering, particularly close to the glacier terminus, results partly from the fact that clastic material of the bottom moraine, being strongly crushed and pulverized, is very reactive. Like other glaciers in the region, the Werenskiold Glacier is a polythermal glacier and thus quite effective in physical erosion of the glacier bed. Apparently, primary minerals are mechanically disintegrated, but not altered much chemically. In contrast to the conclusions of Wadham *et al.* (2010), the biochemical weathering under the ice of the Werenskiold Glacier seems to be insignificant in comparison to the processes accelerated after exposure. Microscopic observation of mineral grains indicates mostly fresh and unaltered surfaces. This may result from a difference between the type of the glacier and may require more detailed studies in future.

The geochemical fates of the metals in question correlate with each other. This is partly a result of geochemical similarities between Fe and Mn as well as between Pb, Zn, and Cu. Additionally, this may reflect the similarities of their primary mineral sources. Iron and manganese result to the large extent from the weathering of carbonates and (alumo)silicates, while the sources of Pb, Zn and Cu are primarily sulphides. Sulphide weathering in the area is evidenced,

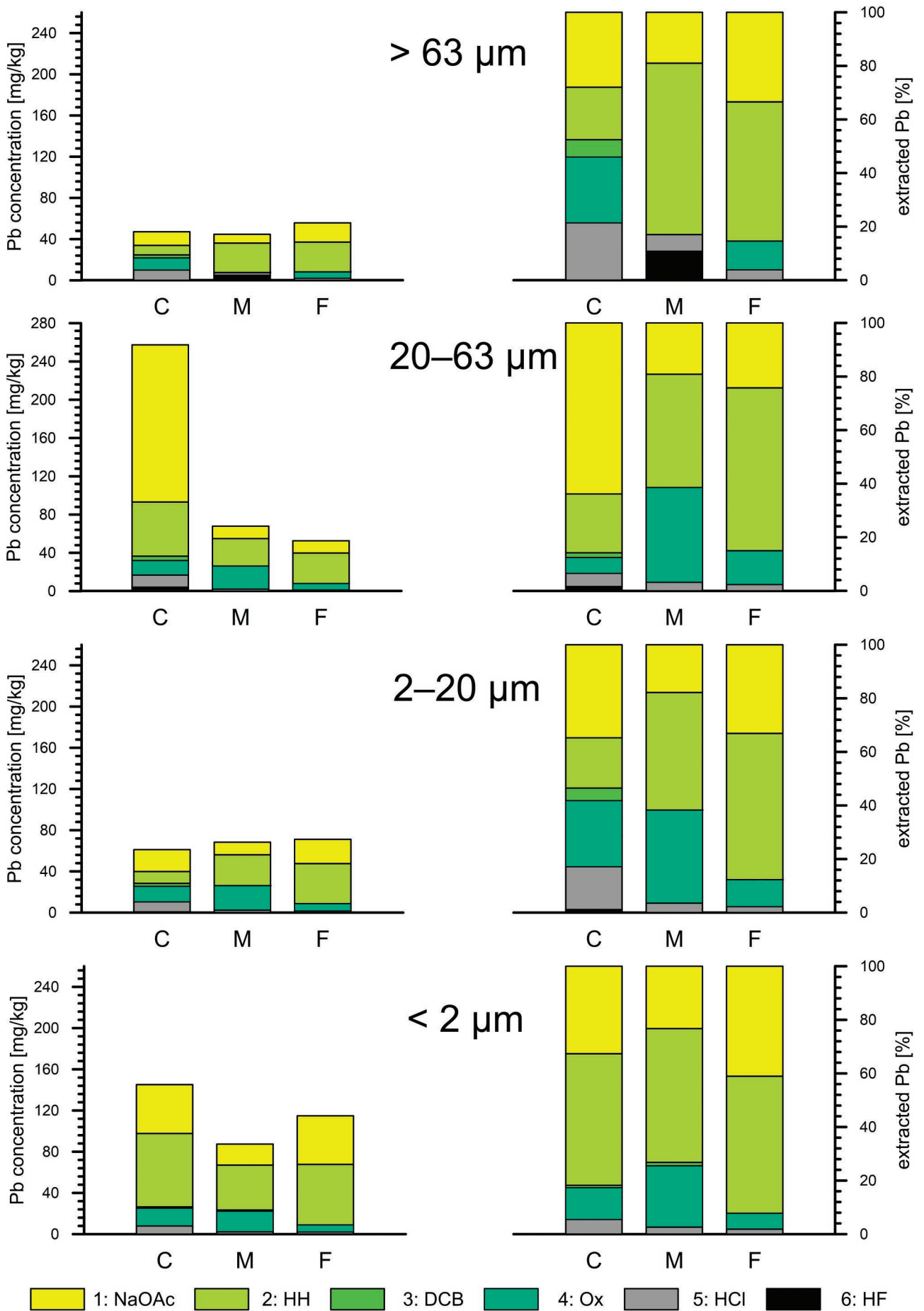


Fig. 10. Lead speciation in various grain fractions of the Werenskioldbreen chronosequence. See Figure 3 for explanations.

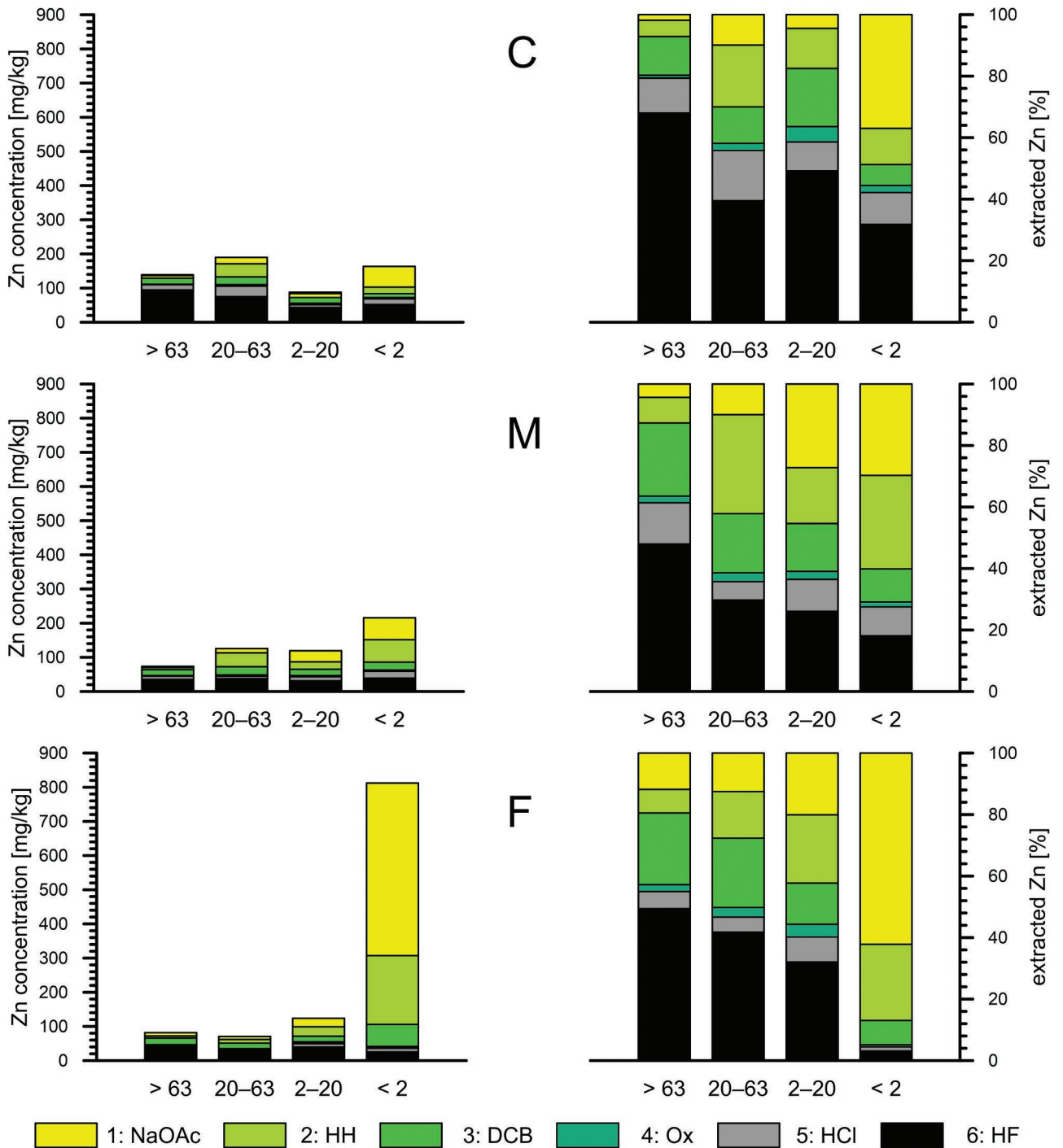


Fig. 11. Zinc speciation in the Werenskioldbreen chronosequence. See Figure 2 for explanations.

among other ways, by direct observations and by sulphur isotope analyses (Szykiewicz *et al.*, 2013).

Very significant is the evolution of mineral speciation, which is common to all the metals studied. The weathering processes dominating the system are: redox reactions and incongruent dissolution, followed by precipitation of the secondary phases and partial sorption of the aqueous species. As a result, the elements released from weathering minerals are only partially transported away from the system. The remaining part transforms by weathering from the coarse-grained fraction (dominated by fragments of prima-

ry minerals) into the fine-grained fraction (in the form of authigenic minerals or as species sorbed on mineral skeleton). This is very pronounced within the chronosequence: the content of all the metals studied correlates identically with the grain size, despite the differences in their chemical character and affinities. Another important observation is a possible relatively rapid transformation of ferrihydrite to more stable iron oxyhydroxides, which obviously affects the bioavailability of iron.

To date, most studies on the denudation rates in the proglacial areas concentrated on the examination of solutions (see

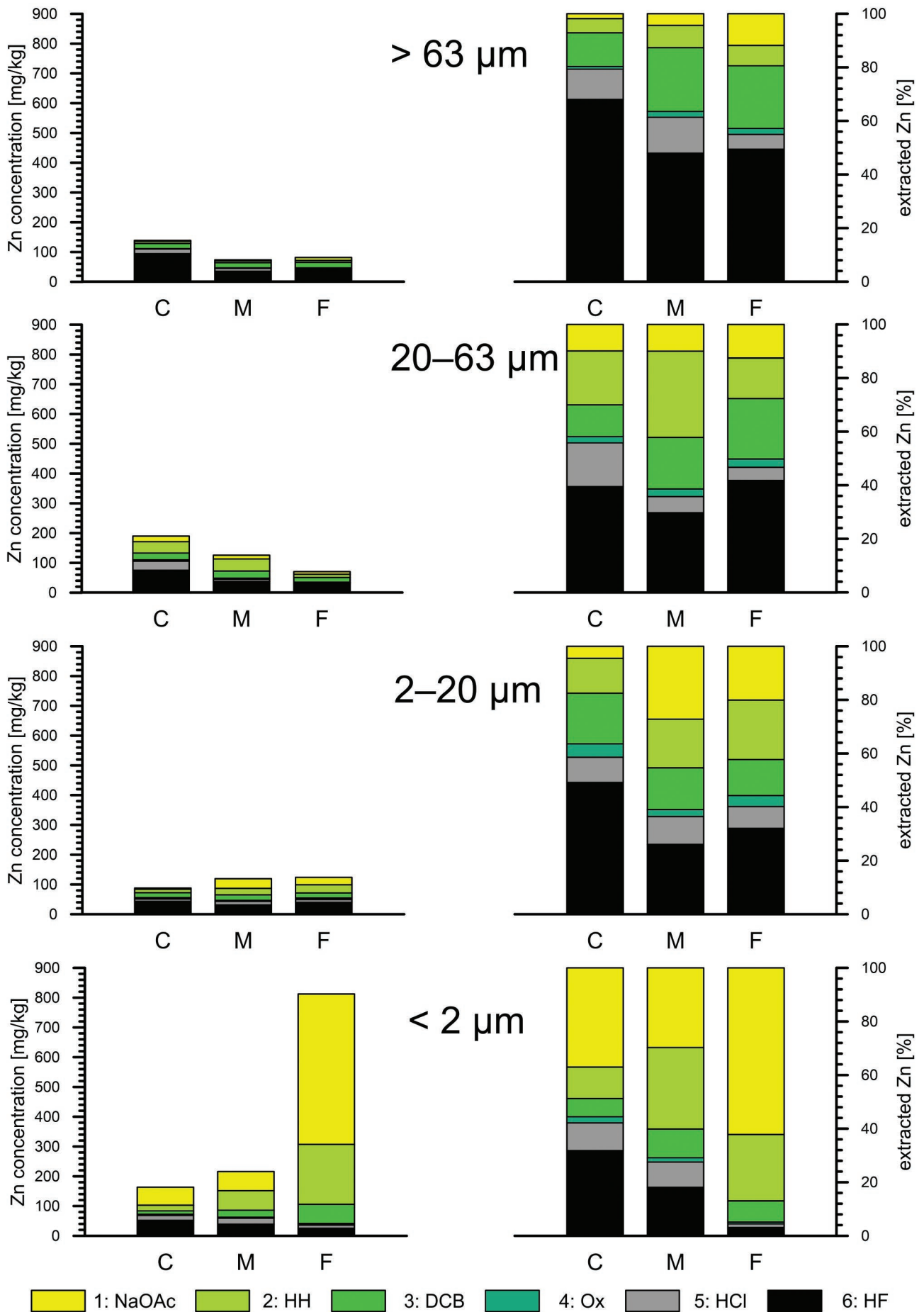


Fig. 12. Zinc speciation in various grain fractions of the Werenskiöldbreen chronosequence. See Figure 3 for explanations.

for example Anderson *et al.*, 2000; Yde *et al.*, 2008; Stachnik *et al.*, 2016 and the literature therein). The mechanisms of weathering, however, cannot be fully inferred only on the basis of indirect macroscopic investigation of the evolution of the composition of solutions. The microscopic study presented herein indicates that the role of incongruent dissolution possibly was underestimated. Also, the formation of coatings of secondary phases was observed on primary mineral surfaces. All these affect the mineral speciation of initial soils as well as the composition of mineral suspensions transported by rivers to the ocean.

For many years, the presence of heavy metals in soils and sediments in Svalbard has been usually linked with air pollution (see for example Grodzińska and Godzik, 1991; Plichta and Kuczyńska, 1991). Direct evidence, however, was never presented and this conclusion was always speculative. Moreover, some studies have suggested that only local sources in the closest vicinity might affect the soil chemistry significantly (Gulińska *et al.*, 2003; Krajcarová *et al.*, 2016; Gonet *et al.*, 2018). The present study indicates that relatively low concentrations of Pb, Zn, and Cu, as well as Fe and Mn determined in surficial sediments and soils may result from natural sulphide and carbonate mineralization, which is quite common there. Therefore, more detailed isotopic studies may be necessary to distinguish natural from anthropogenic sources of these metals, resulting from global and local air and soil pollution.

## CONCLUSIONS

The weathering in the proglacial area of a retreating glacier is very fast. The weathering processes dominating the system are: redox reactions and incongruent dissolution, followed by the precipitation of secondary phases and partial sorption of aqueous species. The geochemical fates of Pb, Zn, and Cu, as well as Fe and Mn, correlate with each other, reflecting a) the geochemical similarities between them, b) the similarities of their primary mineral sources, and c) the significant role of incongruent dissolution. The elements released from weathering minerals are only partially transported away from the system. The remaining part transforms by weathering from a coarse-grained fraction (dominated by fragments of primary minerals) into a fine-grained fraction (in the form of secondary, authigenic minerals or as species sorbed on mineral skeleton). This is very strongly pronounced within the chronosequence: the content of all the metals studied correlates identically with the grain size, despite the differences in their chemical character and affinities. This role of incongruent dissolution previously was underestimated.

The weathering mechanisms observed in the proglacial area of the retreating Werenskiold Glacier are probably representative to the processes in the proglacial areas of glaciers retreating after the glaciations in Europe. Glaciers at Svalbard are not limited to the valley, but through ice-covered passes they form a connected network, which is often closer to the ice cap, rather than to a valley glacier, as in the Alps. This type of ice coverage existed in the Alps during periods of glaciation. Therefore, studies of the chronosequences of a contemporary glacial forefield in the Alps and at Svalbard may provide complementary information.

## Acknowledgements

This work was supported by AGH Research Grant No 16.16.140.315. The authors thank Michał Skiba and Marek Matyjasik, whose constructive comments allowed improvement to the quality and clarity of the manuscript.

## REFERENCES

- Arrigo, K. R., van Dijken, G. L., Castelao, R. M., Luo, H., Rennermalm, Å. K., Tedesco, M., Mote, T. L., Oliver, H. & Yager, P. L., 2017. Melting glaciers stimulate large summer phytoplankton blooms in southwest Greenland waters. *Geophysical Research Letters*, 44: 6278–6285.
- Beaulieu, E., Godderis, Y., Donnadiou, Y., Labat, D. & Roelandt, C., 2012. High sensitivity of the continental-weathering carbon dioxide sink to future climate change. *Nature Climate Change*, 2: 346–349.
- Berner, R. A., Lassaga, A. C. & Garrels, R. M., 1983. The carbon-silicate geochemical cycle and its effect on atmospheric carbon dioxide over the past 100 million years. *American Journal of Science*, 283: 641–683.
- Bhatia, M. P., Kujawinski, E. B., Das, S. B., Breier, C. F., Henderson, P. B. & Charette, M. A., 2013. Greenland meltwater as a significant and potentially bioavailable source of iron to the ocean. *Nature Geoscience*, 6: 274–277.
- Bigham, J. M., Schwertmann, U., Traina, S. J., Winland, R. L. & Wolf, M., 1996. Schwertmannite and the chemical modeling of iron in acid sulfate waters. *Geochimica et Cosmochimica Acta*, 60: 2111–2121.
- Boyd, P. W., Jickells, T., Law, C. S., Blain, S., Boyle, E. A., Bueseler, K. O., Coale, K. H., Cullen, J. J., de Baar, J. W., Follows, M., Harvey, M., Lancelot, C., Levasseur, M., Owens, N. P. J., Pollard, R., Rivkin, R. B., Sarmiento, J., Schoemann, V., Smetacek, V., Takeda, S., Tsuda, A., Turner, S. & Watson, A. J., 2007. Mesoscale iron enrichment experiments 1993–2005: synthesis and future directions. *Science*, 315: 612–617.
- Bukowska-Jania, E., 2003. *The Role of Glacier Systems in the Migration of Calcium Carbonate in the Natural Environment*. Wydawnictwo Uniwersytetu Śląskiego, Katowice, 248 pp. [In Polish, with English summary.]
- Chester, R. & Hughes, M. J., 1967. A chemical technique for the separation of ferro-manganese materials, carbonate minerals and adsorbed trace elements from pelagic sediments. *Chemical Geology*, 2: 249–262.
- Collins, M., Knutti, R., Arblaster, J., Dufresne, J.-L., Fichet, T., Friedligstein, P., Gao, X., Gutowski, W. J. Jr., Johns, T., Krinner, G., Shongwe, M., Tebaldi, C., Weaver, A. J. & Wehner, M., 2013. Long-term climate change: projections, commitments and irreversibility. In: Stocker, T. F., Quin, D., Plattner, G.-K., Tignor, M., Allen, S. K., Boschung, J., Nauels, A., Xia, Y., Bow, V. & Midgley, P. M. (eds), *Climate Change 2013: The Physical Science Basis. Contributions of Working Group I to the Fifth Assessment Report of the Intergovernmental Panel on Climate Change*. Cambridge University Press, Cambridge, pp. 1029–1136.
- Cornell, R. M. & Schwertmann, U., 2003. *The Iron Oxides. Structure, Properties, Reactions, Occurrences, and Uses, 2nd Edition*. Wiley-VCH Verlag GmbH and Co. KGaA, Weinheim, 664 pp.

- Czerny, J., Kieres, A., Manecki, M. & Rajchel, J. (ed.) 1993. *Geological Map of the SW part of Wedel Jarlsberg Land Spitsbergen, 1:25 000*. Institute of Geology and Mineral Deposits, University of Mining and Metallurgy, Kraków.
- Czerny, J., Lipień, G., Manecki, A. & Piestrzyński, A., 1992a. Geology and ore-mineralization of the Hecla Hoek succession (Precambrian) in front of Werenskioldbreen, South Spitsbergen. *Studia Geologica Polonica*, 98: 67–113.
- Czerny, J., Pływacz, I. & Szubała, L., 1992b. Siderite mineralization in the Hecla Hoek Succession (Precambrian) at Strypegga, South Spitsbergen. *Studia Geologica Polonica*, 98: 154–170.
- Dahms, D., Favilli, F., Krebs, R. & Egli, M., 2012. Soil weathering and accumulation rates of oxalate-extractable phases derived from alpine chronosequences up to 1 Ma in age. *Geomorphology*, 151–152: 99–113.
- Death, R., Wadham, J. L., Monteiro, F., Le Brocq, A. M., Tranter, M., Ridgwell, A., Dutkiewicz, S. & Raiswell, R., 2014. Antarctic ice sheet fertilises the Southern Ocean. *Biogeosciences*, 11: 2635–2644.
- Dosseto, A., Vigier, N., Joannes-Boyau, R., Moffat, I., Singh, T. & Srivastava, P., 2015. Rapid response of silicate weathering rates to climate change in Himalaya. *Geochemical Perspectives Letters*, 1: 10–19.
- Douglas, G. B., Hart, B. T., Beckett, R., Gray, C. M. & Oliver, R. L., 1999. Geochemistry of suspended particulate matter (SPM) in the Murray-Darling river system: A conceptual isotopic/geochemical model for the fractionation of major, trace and rare earth elements. *Aquatic Geochemistry*, 5: 167–194.
- Fabri, R. Jr., Krause, M., Dalfior, B. M., Salles, R. C., de Freitas, A. C., da Silva, H. E., Licinio, M. V. V. J., Brandão, G. P. & Carneiro, M. T. W. D., 2018. Trace elements in soil, lichens, and mosses from Fildes Peninsula, Antarctica: spatial distribution and possible origins. *Environmental Earth Sciences*, 77: 124.
- Figura, P., Manecki, M. & Rzepa, G., 2014. Weathering of siderite in the polar conditions. *Geology, Geophysics & Environment*, 40: 84–85.
- Gałęczka, I., Eiriksdóttir, E. S., Hardardóttir, J., Oelkers, E. H., Torssander, P. & Gislason, S. R., 2015. The effect of the 2002 glacial flood on dissolved and suspended chemical fluxes in the Skafta river, Iceland. *Journal of Volcanology and Geothermal Research*, 301: 253–276.
- Gonet, T., Górka-Kostrubiec, B. & Łuczak-Wilamowska, B., 2018. Assessment of topsoil contamination near the Stanisław Siedlecki Polish Polar Station in Hornsund, Svalbard, using magnetic methods. *Polar Science*, 15: 75–86.
- Górniak, D., Marszałek, H., Kwaśniak-Kominek, M., Rzepa, G. & Manecki, M., 2017. Soil formation and initial microbiological activity on a foreland of an Arctic glacier (SW Svalbard). *Applied Soil Ecology*, 114: 34–44.
- Grodzińska, K. & Godzik, B., 1991. Heavy metals and sulphur in mosses from southern Spitsbergen. *Polar Research*, 9: 133–140.
- Gulińska, J., Rachlewicz, G., Szczuciński, W., Barałkiewicz, D., Kózka, M., Bulska, E. & Burzyk, M., 2003. Soil contamination in High Arctic areas of human impact, Central Spitsbergen, Svalbard. *Polish Journal of Environmental Studies*, 12: 701–707.
- Hagen, J. O., Liestol, O., Roland, E. & Jorgensen, T., 1993. *Glacier Atlas of Svalbard and Jan Mayen*. Meddeleser Nr. 129. Norsk Polarinstittutt, Oslo, 143 pp.
- Hawking, J. R., Benning, L. G., Raiswell, R., Kaulich, B., Araki, T., Abyaneh, M., Stockdale, A., Koch-Müller, M., Wadham, J. L. & Tranter, M., 2018. Biolabile ferrous iron bearing nanoparticles in glacial sediments. *Earth and Planetary Science Letters*, 493: 92–101.
- Hawking, J. R., Wadham, J. L., Benning, L. G., Hendry, K. R., Tranter, M., Tedstone, A., Nienow, P. & Raiswell, R., 2017. Ice sheets as a missing source of silica to the polar oceans. *Nature Communications*, 8: 14198.
- Hawking, J. R., Wadham, J. L., Tranter, M., Lawson, E., Sole, A., Cowton, T., Tedstone, A. J., Bartholomew, I., Nienow, P., Chandler, D. & Telling, J., 2015. The effect of warming climate on nutrient and solute export from the Greenland Ice Sheet. *Geochemical Perspectives Letters*, 1: 94–104.
- Hawking, J. R., Wadham, J. L., Tranter, M., Raiswell, R., Benning, L. G., Statham, P. J., Tedstone, A., Nienow, P., Lee, K. & Telling, J., 2014. Ice sheets as a significant source of highly reactive nanoparticulate iron to the oceans. *Nature Communications*, 5: 3929.
- He, L. & Tang, Y., 2008. Soil development along primary succession sequences on moraines of Hailuoguo Glacier, Gongga Mountain, Sichuan, China. *Catena*, 72: 259–269.
- Hiemstra, T., 2015. Formation, stability, and solubility of metal oxide nanoparticles: surface entropy, enthalpy, and free energy of ferrihydrite. *Geochimica et Cosmochimica Acta*, 158: 179–198.
- Hirst, C., Andersson, P. S., Shaw, S., Burke, I. T., Kutcher, L., Murphy, M. J., Maximov, T., Pokrovsky, O. S., Mörth, C-M. & Porcelli, D., 2017. Characterisation of Fe-bearing particles and colloids in the Lena River basin, NE Russia. *Geochimica et Cosmochimica Acta*, 213: 553–573.
- Ignatiuk, D. & Migąła, K., 2013. Werenskiold glacier. In: Zwoliński, Z., Kostrzewski, A., Pulina, M. (eds), *Ancient and Modern Geoecosystems of Spitsbergen*. Association of Polish Geomorphologists, Poznań, pp. 96–99.
- Kabała, C. & Zapart, J., 2009. Recent, relic and buried soils in the forefield of Werenskiold Glacier, SW Spitsbergen. *Polish Polar Research*, 30: 161–178.
- Kabała, C. & Zapart, J., 2012. Initial soil development and carbon accumulation on moraines of the rapidly retreating Werenskiold Glacier, SW Spitsbergen, Svalbard archipelago. *Geoderma*, 175–176: 9–20.
- Kiczka, M., Wiederhold, J. G., Frommer, J., Voegelin, A., Kraemer, S. M., Bourdon, B. & Kretzschmar, R., 2011. Iron speciation and isotope fractionation during silicate weathering and soil formation in an alpine glacier forefield chronosequences. *Geochimica et Cosmochimica Acta*, 75: 5559–5573.
- Kieres, A. & Piestrzyński, A., 1992. Ore-mineralization of the Hecla Hoek succession (Precambrian) around Werenskioldbreen, South Spitsbergen. *Studia Geologica Polonica*, 98: 116–151.
- Kowalska, A. & Sroka, W., 2008. Sedimentary environment of the Nottinghambukta delta, SW Spitsbergen. *Polish Polar Research*, 29: 245–259.
- Krajcarová, L., Novotný, K., Chattová, B. & Elster, J., 2016. Elemental analysis of soils and *Salix polaris* in the town of Pyramiden and its surroundings (Svalbard). *Environmental Science and Pollution Research*, 23: 10124–10137.
- Kwaśniak-Kominek, M., Manecki, M., Rzepa, G., Płonka, A. & Górniak, D., 2016. Weathering in a regolith on the Werenskioldbreen glacier forefield (SW Spitsbergen): Modeling of

- pore water chemistry. *Annales Societatis Geologorum Polonicae*, 86: 249–264.
- Laska, M., Barzycka, B. & Luks, B., 2017. Melting characteristics of snow cover on tidewater glaciers in Hornsund Fjord, Svalbard. *Water*, 9: 804.
- Liu, X. & Millero, F. J., 2002. The solubility of iron in seawater. *Marine Chemistry*, 7: 43–54.
- Majchrowska, E., Ignatiuk, D., Jania, J., Marszałek, H. & Wąsik, M., 2015. Seasonal and interannual variability in runoff from the Werenskioldbreen catchment, Spitsbergen. *Polish Polar Research*, 36: 197–224.
- Majka, J., Be'eri-Shlevin, Y., Gee, D. G., Czerny, J., Frei, D. & Ladenberger, A., 2013. Torellian (c. 640 Ma) metamorphic overprint of the Tonian (c. 950Ma) basement in the Caledonides of southwestern Svalbard. *Geological Magazine*, 151: 732–748.
- Majka, J., Czerny, J., Mazur, S., Holm, D. K. & Manecki, M., 2010. Neoproterozoic metamorphic evolution of the Isbjørnhamna Group rocks from south-western Svalbard. *Polar Research*, 29: 250–264.
- Majka, J., Mazur, S., Manecki, M., Czerny, J. & Holm, D. K., 2008. Late Neoproterozoic amphibolite facies metamorphism of a pre-Caledonian basement block in southwest Wedel Jarlsberg Land, Spitsbergen: new evidence from U-Th-Pb dating of monazite. *Geological Magazine*, 145: 822–830.
- Maneck, M., Holm, D. K., Czerny, J. & Lux, D., 1998. Thermochronological evidence for late Proterozoic (Vendian) cooling in southwest Wedel Jarlsberg Land, Spitsbergen. *Geological Magazine*, 135: 63–69.
- Mapelli, F., Marasco, R., Fusi, M., Scaglia, B., Tsiamis, G., Rolli, E., Fodelianakis, S., Bourtzis, K., Ventura, S., Tambone, F., Adani, F., Borin, S. & Daffonchio, D., 2018. The stage of soil development modulates rhizosphere effect along a High Arctic desert chronosequence. *The ISME Journal*, 12: 1188–1198.
- Marsz, A. A. & Styszyńska, A. (eds), 2013. *Climate and Climate Change at Hornsund, Svalbard*. Gdynia Maritime University, Gdynia, 402 pp.
- Marszałek, H. & Górniak, D., 2017. Changes in water chemistry along the newly formed High Arctic fluvial-lacustrine system of the Bratæg Valley (SW Spitsbergen, Svalbard). *Environmental Earth Science*, 76: 449.
- Martinez-Garcia, A., Sigman, D. M., Ren, H., Anderson, R. F., Straub, M., Hodell, D. A., Jaccard, S. L., Eglinton, T. I. & Haug, G. H., 2014. Iron fertilization of the Subantarctic Ocean during the last ice age. *Science*, 343: 1347–1350.
- Mavris, C., Egli, M., Plötze, M., Blum, J. D., Mirabella, A., Giaccai, D. & Haeberli, W., 2010. Initial stages of weathering and soil formation in the Morteratsch proglacial area (Upper Engadine, Switzerland). *Geoderma*, 155: 359–371.
- Mavris, C., Plötze, M., Mirabella, A., Giaccai, D., Valboa, G. & Egli, M., 2011. Clay mineral evolution along a soil chronosequence in an Alpine proglacial area. *Geoderma*, 165: 106–117.
- Mehra, O. P. & Jackson, M. L., 1960. Iron oxide removal from soils and clays by a dithionite-citrate system buffered with sodium bicarbonate. *Clays and Clay Minerals*, 7: 317–327.
- Melke, J., 2006. The contents of selected trace elements in the soils of Bellsund, Spitsbergen. *Polish Journal of Soil Science*, 39: 21–32.
- Melke, J. & Chodorowski, J. 2006. Formation of Arctic soils in Chamberlindalen, Bellsund, Spitsbergen. *Polish Polar Research*, 27: 119–132.
- Meyer, C. R. & Minchew, B. M., 2018. Temperate ice in the shear margins of the Antarctic Ice Sheet: Controlling processes and preliminary locations. *Earth and Planetary Science Letters*, 498: 17–26.
- Moskovchenko, D. V., Kurchatova, A. N., Fefilov, N. N. & Yurtaev, A. A., 2017. Concentrations of trace elements and iron in the Arctic soils of Belyi Island (the Kara Sea, Russia): patterns of variation across landscapes. *Environmental Monitoring and Assessment*, 189: 210.
- Olichwer, T., Tarka, R. & Modelska, M., 2013. Chemical composition of groundwaters in the Hornsund region, southern Spitsbergen. *Hydrology Research*, 44: 117–130.
- Olsen, M. S., Callaghan, T. V., Reist, J. D., Reiersen, L. O., Dahl-Jensen, D., Granskog, M. A., Goodison, B., Hovelsrud, G. K., Johansson, M., Kallenborn, R., Key, J., Klepikov, A., Meier, W., Overland, J. E., Prowse, T. D., Sharp, M., Vincent, W. F. & Walsh, J., 2011. The changing Arctic cryosphere and likely consequences: an overview. *AMBIO*, 40: 111–118.
- Osuch, M. & Wawrzyniak, T., 2016. Climate projections in the Hornsund area, Southern Spitsbergen. *Polish Polar Research*, 37: 379–402.
- Overeem, I., Hudson, B. D., Syvitski, J. P. M., Mikkelsen, A. B., Hasholt, B., van den Broeke, M. R., Noël, B. P. Y. & Morlighem, M., 2017. Substantial export of suspended sediment to the global oceans from glacial erosion in Greenland. *Nature Geoscience*, 10: 859–863.
- Pachauri, R. J., Meyer, L. & The Core Writing Team, 2014. *Climate Change 2014: Synthesis Report*. [http://ipcc.ch/pdf/assessment-report/ar5/syr/SYR\\_AR5\\_FINAL\\_full\\_wcover.pdf](http://ipcc.ch/pdf/assessment-report/ar5/syr/SYR_AR5_FINAL_full_wcover.pdf)
- Pälli, A., Moore, J. C., Jania, J., Kolondra, L. & Głowacki, P., 2003. The drainage pattern of Hansbreen and Werenskioldbreen, two polythermal glaciers in Svalbard. *Polar Research*, 22: 355–371.
- Pirożnikow, E. & Górniak, A., 1992. Changes in the characteristics of the soil and vegetation during the primary succession in the marginal zone of the Werenskiold glacier, Spitsbergen. *Polish Polar Research*, 13: 19–29.
- Plichta, W. & Kuczyńska, I., 1991. Metal contents in soils of Kafliøyra, Spitsbergen. *Polish Polar Research*, 12: 183–193.
- Poulton, S. W. & Canfield, D. E., 2005. Development of a sequential extraction procedure for iron: implications for iron partitioning in continentally derived particulates. *Chemical Geology*, 214: 209–221.
- Poulton, S. W. & Raiswell, R., 2002. The low-temperature geochemical cycle of iron: from continental fluxes to marine sediment deposition. *American Journal of Science*, 302: 774–805.
- Poulton, S. W. & Raiswell, R., 2005. Chemical and physical characteristics of iron oxides in riverine and glacial meltwater sediments. *Chemical Geology*, 218: 203–221.
- Raiswell, R., 2011a. Iron transport from the continents to the open ocean: the aging-rejuvenation cycle. *Elements*, 7: 101–106.
- Raiswell, R., 2011b. Iceberg-hosted nanoparticulate Fe in the Southern Ocean: Mineralogy, origin, dissolution kinetics and source of bioavailable Fe. *Deep Sea Research II*, 58: 1364–1375.
- Raiswell, R., Benning, L. G., Davidson, L. & Tranter, M., 2008. Nanoparticulate bioavailable iron minerals in icebergs and glaciers. *Mineralogical Magazine*, 72: 345–348.
- Raiswell, R., Benning, L. G., Davidson, L., Tranter, M. & Tulaczyk, S., 2009. Schwertmannite in wet, acid, and oxic

- microenvironments beneath polar and polythermal glaciers. *Geology*, 37: 431–434.
- Raiswell, R. & Canfield, D. E., 2012. The iron biogeochemical cycle past and present. *Geochemical Perspectives*, 1: 1–220.
- Raiswell, R., Canfield, D. E. & Berner, R. A., 1994. A comparison of iron extraction methods for the determination of degree of pyritization and recognition of iron-limited pyrite formation. *Chemical Geology*, 111: 101–111.
- Raiswell, R., Hawking, J. R., Benning, L. G., Baker, A. R., Death, R., Albani, S., Mahowald, N., Krom, M. D., Poulton, S. W., Wadhwa, J. & Tranter, M., 2016. Potentially bioavailable iron delivery by iceberg-hosted sediments and atmospheric dust to the polar oceans. *Biogeosciences*, 13: 3887–3900.
- Raiswell, R., Tranter, M., Benning, L. G., Siegert, M., De'ath, R., Huybrechts, P. & Payne, T., 2006. Contributions from glacially derived sediment to the global iron (oxyhydr)oxide cycle: Implications for iron delivery to the oceans. *Geochimica et Cosmochimica Acta*, 70: 2765–2780.
- Regenspurg, S., Brand, A. & Peiffer, S., 2004. Formation and stability of schwertmannite in acidic mining lakes. *Geochimica et Cosmochimica Acta*, 68: 1185–1197.
- Reinardy, B. T. I., Booth, A. D., Hughes, A. L. C., Boston, C. M., Åkesson, H., Bakke, J., Nesje, A., Giesen, R. H. & Pearce, D. M., 2019. Pervasive cold ice within a temperate glacier – implications for glacier thermal regimes, sediment transport and foreland geomorphology. *The Cryosphere*, 13: 827–843.
- Righi, D., Huber, K. & Keller, C., 1999. Clay formation and podzol development from postglacial moraines in Switzerland. *Clay Minerals*, 34: 319–332.
- Ross, K. W. & Wang, J., 1993. Extractable Al, Fe, Mn and Si. In: Carter, M. R. (ed.), *Soil Sampling and Methods of Analysis*. Lewis Publishers, pp. 239–246.
- Rysgaard, S., Mortensen, J., Juul-Pedersen, T., Sørensen, L. L., Lennert, K., Søggard, D. H., Andert, K. E., Blicher, M. E., Sej, M. K. & Bendtsen, J., 2012. High air-sea uptake rates in nearshore and shelf areas of Southern Greenland: temporal and spatial variability. *Marine Chemistry*, 128–129: 26–33.
- Rzepa, G., Bajda, T. & Sikora, M., 2006. Speciation and concentration of trace elements in the ferruginous sediments of Poland. *Polish Journal of Environmental Studies*, 15, 2a: 474–478.
- Sharp, M. & Tranter, M., 2017. Glacier biogeochemistry. *Geochemical Perspectives*, 6, 2: 1–340.
- Shepherd, A., Ivins, E. R., Geruo, A., Barletta, V. R., Bentley, M. J., Bettadpur, S., Briggs, K. H., Bromwich, D. H., Forsberg, R., Galin, N., Horwath, M., Jacob, S., Joughin, I., King, M. A., Lenaerts, J. T. M., Li, J., Ligtenberg, S. R. M., Luckman, A., Luthcke, S. B., McMillan, M., Meister, R., Milne, G., Mouginout, J., Muir, A., Nicolas, J. P., Paden, J., Payne, A. J., Pritchard, H., Rignot, E., Rott, H., Sørensen, L. S., Scambos, T. A., Scheuchl, B., Schrama, E. J. O., Smith, B., Sundal, A. V., van Angelen, J. H., van de Berg, W. J., van den Broeke, M. R., Vaughan, D. G., Velicogna, I., Wahr, J., Whitehouse, P. L., Wingham, D. J., Yi, D., Young, D. & Zwally, H. J., 2012. A reconciled estimate of ice sheet mass balance. *Science*, 338: 1183–1189.
- Shoenfelt, E. M., Sun, J., Winckler, G., Kaplan, M. R., Borunda, A. L., Farrell, K. R., Moreno, P. I., Gaiero, D. M., Recasens, C., Sambrotto, R. N. & Bostick, B. C., 2017. High particulate iron(II) content in glacially sourced dusts enhances productivity of a model diatom. *Science Advances*, 3: e1700314.
- Singh, A. K., Hasnain, S. I. & Banerjee, D. K., 1999. Grain size and geochemical partitioning of heavy metals of the Damodar River – a tributary of the lower Ganga, India. *Environmental Geology*, 39: 90–98.
- Skiba, S., Drewnik, M. & Kacprzak, A., 2002. Soils of the western coast of Sörkappland. In: Ziaja, W. & Skiba, S. (eds), *Sörkappland Landscape Structure and Functioning (Spitsbergen, Svalbard)*. Wydawnictwo Uniwersytetu Jagiellońskiego, Kraków, pp. 51–86.
- Sobota, I., 2016. Icings and their role as an important element of the cryosphere in High Arctic glacier forefields. *Bulletin of Geography, Physical Geography Series*, 10: 81–93.
- Stachnik, Ł., Majchrowska, E., Yde, J. C., Nawrot, A. P., Cichała-Kamrowska, K., Ignatiuk, D. & Piechota, A., 2016. Chemical denudation and the role of sulfide oxidation at Werenskioldbreen, Svalbard. *Journal of Hydrology*, 538: 177–173.
- Szymański, W., Siwek, J., Waścińska, J. & Wojtuń, B., 2016. Texture and geochemistry of surface horizons of Arctic soils from a non-glaciated catchment, SW Spitsbergen. *Polish Polar Research*, 37: 361–377.
- Szymański, W., Skiba, S. & Wojtuń, B., 2013. Distribution, genesis and properties of Arctic soils: a case study from the Fuglebekken catchment, Spitsbergen. *Polish Polar Research*, 34: 289–304.
- Szymański, W., Skiba, M., Wojtuń, B. & Drewnik, M., 2015. Soil properties, micromorphology, and mineralogy of Cryosols from sorted and unsorted patterned grounds in the Hornsund area, SW Spitsbergen. *Geoderma*, 253–254: 1–11.
- Szynkiewicz, A., Modelska, M., Buczyński, S., Borrok, D. M. & Merrison, J. P., 2013. The polar sulfur cycle in the Werenskioldbreen, Spitsbergen: Possible implications of understanding the deposition of sulfate minerals in the North Polar Region of Mars. *Geochimica et Cosmochimica Acta*, 106: 326–343.
- Taylor, K. G. & Konhauser, K. O., 2011. Iron in Earth surface systems: a major player in chemical and biological processes. *Elements*, 7: 83–88.
- Taylor, L. L., Quirk, J., Thorley, R. M. S., Kharecha, P. A., Hansen, J., Ridgwell, A., Lomas, M. R., Banwart, S. A. & Beerling, D. J., 2016. Enhanced weathering strategies for stabilizing climate and averting ocean acidification. *Nature Climate Change*, 6: 402–408.
- Tessier, A., Campbell, P. G. C. & Bisson, M., 1979. Sequential extraction for the speciation of particulate trace metals. *Analytical Chemistry*, 51: 844–851.
- Wadhwa, J. L., De'ath, R., Monteiro, F. M., Tranter, M., Ridgwell, A., Raiswell, R. & Tulaczyk, S., 2013. The potential role of the Antarctic Ice Sheet in global biogeochemical cycles. *Earth and Environmental Science Transactions of the Royal Society of Edinburgh*, 10: 1–13.
- Wadhwa, J. L., Tranter, M., Skidmore, M., Hodson, A. J., Priscu, J., Lyons, W. B., Sharp, M., Wynn, P. & Jackson, M., 2010. Biogeochemical weathering under ice: Size matters. *Global Biogeochemical Cycles*, 24: GB3025.
- Walker, J. C. G., Hays, P. B. & Kasting, J. F., 1981. A negative feedback mechanism for the long-term stabilization of Earth's surface temperature. *Journal of Geophysical Research*, 86: 9776–9782.
- Wojcik, R., Donhauser, J., Holm, S., Malard, L., Holland, A., Frey, B., Wagner, D., Pearce, D., Anesio, A., Hövelmann, J. & Benning, L. G., 2017. Geochemical and microbiological succes-

- sion patterns in a High-Arctic proglacial area. *Goldschmidt Conference, Paris*. DOI: 10.13140/RG.2.2.15750.06723.
- Yde, J. C., Riger-Kusk, M., Christiansen, H. H., Knudsen, N. T. & Humlum, O., 2008. Hydrochemical characteristics of bulk meltwater from the entire ablation season, Longyerbreen, Svalbard. *Journal of Glaciology*, 54: 259–272.
- Zaborska, A., Beszczyńska-Möller, A. & Włodarska-Kowalczyk, M., 2017. History of heavy metal accumulation in the Svalbard area: Distribution, origin and transport pathways. *Environmental Pollution*, 231: 437–450.
- Zemp, M., Frey, H., Gärtner-Roer, I., Nussbaumer, S. U., Hoelzle, M., Paul, F., Haeberli, W., Denzinger, F., Ahlstrøm, A. P., Anderson, B., Bajracharya, S., Baroni, C., Braun, L. N., Cáceres, B. E., Cassaya, G., Cobos, G., Dávila, L. R., Delgado Granados, H., Demuth, M. N., Espizua, L., Fischer, A., Fujita, K., Gadek, B., Ghazanfar, A., Hagen, J. O., Holmlund, P., Karimi, N., Li, Z., Pelto, M., Pitte, P., Popovnin, V. V., Portocarrero, C. A., Prinz, R., Sangewar, C. V., Severskiy, I., Sigurdsson, O., Soruco, A., Usubaliev, R. & Vincent, C., 2015. Historically unprecedented global glacier decline in the early 21st century. *Journal of Glaciology*, 61: 745–762.
- Zhang, Z., Bi, X., Li, X., Zhao, Q. & Chen, H., 2018. Schwertmannite: occurrence, properties, synthesis and application in environmental remediation. *RSC Advances*, 8: 33583–33599.
- Zwoliński, Z., Giżejowski, J., Karczewski, A., Kasprzak, M., Lankauf, K. R., Migoń, P., Pękala, K., Repelewska-Pękalowa, J., Rachlewicz, G., Sobota, I., Stankowski, W. & Zagórski, P., 2013. Geomorphological settings of Polish research areas on Spitsbergen. *Landform Analysis*, 22: 125–143.

